

MACHINING OF POLYCARBONATE FOR OPTICAL APPLICATIONS

A THESIS SUBMITTED TO
THE GRADUATE SCHOOL OF NATURAL AND APPLIED SCIENCES
OF
MIDDLE EAST TECHNICAL UNIVERSITY

BY

MÜSLÜM BOLAT

IN PARTIAL FULFILLMENT OF THE REQUIREMENTS
FOR
THE DEGREE OF MASTER OF SCIENCE
IN
MECHANICAL ENGINEERING

SEPTEMBER 2013

Approval of the thesis:

MACHINING OF POLYCARBONATE FOR OPTICAL APPLICATIONS

submitted by **MÜSLÜM BOLAT** in partial fulfillment of the requirements for the degree of **Master of Science in Mechanical Engineering Department, Middle East Technical University** by,

Prof. Dr. Canan Özgen
Dean, Graduate School of **Natural and Applied Sciences**

Prof. Dr. Suha Oral
Head of the Department, **Mechanical Engineering**

Prof. Dr. M. A. Sahir Arıkan
Supervisor, **Mechanical Engineering Dept., METU**

Examining Committee Members:

Prof. Dr. Mustafa İlhan Gökler
Mechanical Engineering Dept., METU

Prof. Dr. M. A. Sahir Arıkan
Mechanical Engineering Dept., METU

Prof. Dr. Tuna Balkan
Mechanical Engineering Dept., METU

Prof. Dr. Can Çoğun
Mechanical Engineering Dept., Çankaya University

Onat Totuk, M.Sc.
Mechanical Engineering Dept., Çankaya University

Date: 03.09.2013

I hereby declare that all information in this document has been obtained and presented in accordance with academic rules and ethical conduct. I also declare that, as required by these rules and conduct, I have fully cited and referenced all material and results that are not original to this work.

Name, Last Name : Müslüm BOLAT

Signature :

ABSTRACT

MACHINING OF POLYCARBONATE FOR OPTICAL APPLICATIONS

Bolat, Müslüm

M.Sc., Department of Mechanical Engineering

Supervisor: Prof. Dr. M. A. Sahir Arıkan

September 2013, 94 pages

Polycarbonate is a very strong and durable material, highly transparent to visible light, with superior light transmission compared to many kinds of glass. Due to its superior properties, polycarbonate is one of the most common materials used in optical applications. Since surface quality is the main issue for optical performance, optimum cutting conditions should be examined to achieve the best surface quality.

In this thesis, the effects of cutting parameters and vibration on product quality are experimentally studied. Polycarbonate specimens are machined by Single Point Diamond Turning machine and the roughness values of the diamond turned surfaces are measured by White Light Interferometer. A Bruel & Kjaer 4524B accelerometer is used to gather vibration data. Optimum cutting conditions are investigated by three-level full factorial design and an empirical formula is obtained to determine the surface roughness by considering feed rate, depth of cut and spindle speed. Artificial Neural Network (ANN) modeling is also implemented to predict the surface roughness for different cutting conditions.

During experiments, the best average surface roughness value is achieved as 2.7 nm which greatly satisfies the demand for optical quality.

Keywords: Polycarbonate, Single Point Diamond Turning, Monocrystalline Diamond Tool, Surface Roughness, Vibration

ÖZ

POLİKARBONATIN OPTİK UYGULAMALAR İÇİN İŞLENMESİ

Bolat, Müslüm

Yüksek Lisans, Makina Mühendisliği Bölümü

Tez Yöneticisi: Prof. Dr. M. A. Sahir Arıkan

Eylül 2013, 94 sayfa

Polikarbonat, birçok cam türüne göre üstün ışık geçirgenliğine sahip, görünür ışık için son derece şeffaf, çok güçlü ve dayanıklı bir malzemedir. Polikarbonat, bu üstün özellikleri nedeniyle, optik uygulamalarda en yaygın kullanılan malzemelerden biridir. Yüzey kalitesinin optik performans için ana unsurlardan biri olması nedeniyle, en iyi yüzey kalitesini elde etmek için kullanılması gereken optimum kesme deneysel olarak incelenmiştir.

Polikarbonat örnekleri elmas uçlu torna ile işlenmiş ve yüzey pürüzlülüğü Beyaz Işık İnterferometresi ile ölçülmüştür. Bruel&Kjaer 4524B türü ivmeölçer titreşim ölçümlerinde kullanılmıştır. Optimum kesme koşulları tam faktöriyel deneysel çalışma methodu ile incelenmiş ve yüzey pürüzlülüğü için matematiksel formül, ilerleme hızı, kesme derinliği ve aksel hız kullanılarak hesaplanmıştır. Yapay Sinir Ağı modelleme tekniği, farklı kesim koşullarında yüzey pürüzlülüğünü tahmin etmek için kullanılmıştır.

Deneyler sonucunda, en iyi ortalama yüzey pürüzlülüğü değeri, optik kalite talebini büyük ölçüde karşılayan 2.7 nm olarak ölçülmüştür.

Anahtar Kelimeler: Polikarbonat, Elmas Uçlu Tornalama, Monokristal Elmas Takım, Yüzey Pürüzlülüğü, Titreşim

To My Family

ACKNOWLEDGEMENTS

The author would like to express his gratitude to his thesis supervisor Prof. Dr. M. A. Sahir ARIKAN for his guidance, advise, encouragements and helpful criticism throughout the research.

The author would like to thank to Prof. Dr. Mustafa İlhan GÖKLER, Prof. Dr. Tuna BALKAN, Prof. Dr. Can ÇOĞUN and Mr. Onat TOTUK for their helpful comments during thesis defense.

The author wished to express his sincere appreciation to ASELSAN, Inc. and his manager in ASELSAN, Mr. İhsan ÖZSOY, for his support and providing the facility in his study and let to use Single Point Diamond Turning Machine also by the author with encouragement. The author also has to thank to Mr. Tolga Ziya SANDER and Mr. Çağlar YERGÖK for their valuable and beneficial supports and useful comments during the study.

The author would like to thank to technical assistance of Mr. İlker SEZEN for operation of the Single Point Diamond Turning Machine.

The author also would like to thank Mr. Taner KALAYCIOĞLU and Mr. Güvenç CANBALOĞLU for their help during the preparation of vibration test setup.

The author wishes to offer his deepest thanks to his pregnant wife who supported him throughout the entire research.

TABLE OF CONTENTS

ABSTRACT.....	v
ÖZ	vi
ACKNOWLEDGEMENTS	viii
TABLE OF CONTENTS.....	ix
LIST OF TABLES	xii
LIST OF FIGURES	xiv
LIST OF SYMBOLS	xvii
LIST OF ABBREVIATIONS	xviii
CHAPTERS	
1 INTRODUCTION	1
1.1 Motivation.....	1
1.2 Surface Finish and Optical Quality	3
1.3 Machining of Plastics and Polycarbonate	6
1.4 Aim and Scope of Thesis	8
2 LITERATURE SURVEY	11
2.1 Introduction.....	11
2.2 Wear Mechanisms During Cutting Plastics	12
2.3 Effect of Material Characteristics on Surface Roughness.....	13
2.4 Effect of Temperature on Surface Roughness	14
2.5 Effect of Vibration on Surface Roughness.....	15
2.6 Optimization of Parameters Affecting Surface Roughness.....	16

3	DESIGN OF EXPERIMENTS, EXPERIMENT PROCEDURE AND RESULTS	19
3.1	Introduction.....	19
3.2	Experimental Design.....	19
3.2.1	Three Level Full Factorial Design	20
3.2.2	Artificial Neural Network Approach	22
3.3	Single Point Diamond Turning	23
3.4	Mono-crystalline Diamond Tool Setup	25
3.5	Vibration Data Collection Setup.....	26
3.6	Work-piece Setup	29
3.7	Surface Roughness Measurement	32
3.8	Machining Parameters and Experimental Procedure	34
3.9	Three-Level Full Factorial Design.....	36
3.10	Artificial Neural Network Modeling	45
3.11	Comparison of Experimental Methods	52
3.12	Repeatability of the Experiment	54
4	INTERPRETATION OF EXPERIMENTAL RESULTS.....	57
4.1	Introduction.....	57
4.2	Effect of Feed Rate	57
4.3	Effect of Depth of Cut	60
4.4	Effect of Spindle Speed	61
4.5	Effect of Vibration	63
5	DISCUSSION AND CONCLUSION.....	67
5.1	Future Work.....	68
	REFERENCES	69
	APPENDICES	
A	SURFACE ROUGHNESS PARAMETERS	75

B	TECHNICAL SPECIFICATIONS OF SINGLE POINT DIAMOND TURNING MACHINE.....	77
C	TOOL NUMBERING SYSTEM OF CONTOUR FINE TOOLING COMPANY	79
D	PRODUCT DATA SHEET FOR POLYCARBONATE.....	81
E	TECHNICAL SPECIFICATIONS OF WHITE LIGHT INTERFEROMETRY	83
F	SURFACE ROUGHNESS MEASUREMENTS	85
G	ALL SURFACE ROUGHNESS MEASUREMENTS FOR 27-RUNS TESTING EXPERIMENT	89
H	ALL SURFACE ROUGHNESS MEASUREMENTS FOR 8-RUNS VALIDATION EXPERIMENT	95

LIST OF TABLES

TABLES

Table 1-1 Estimated temperature rise by Smith [12]	7
Table 2-1 The best achieved surface roughness values during the diamond turning of polycarbonate in literature	18
Table 3-1 Design of Experiments Methods [58].....	20
Table 3-2 Runs for Three-level Full Factorial Design with Three Parameters.....	21
Table 3-3 Machining Parameters for Experiment 1	36
Table 3-4 Order of Runs for the Experiment 1	37
Table 3-5 Results of the Surface Roughness Measurements for Experiment 1	38
Table 3-6 The coefficients for 3^3 full factorial design	40
Table 3-7 Comparison of measured and predicted R_a values.....	42
Table 3-8 Comparison of measured and predicted R_q and PV values	43
Table 3-9 Summary of Fit.....	44
Table 3-10 ANOVA for prediction model.....	44
Table 3-11 F-Test for factors	45
Table 3-12 Descriptive Statistics for Vibration and Surface Roughness	45
Table 3-13 Pearson's Correlations for Vibration Data	46
Table 3-14 Pearson's Correlations for Cutting Parameters	47
Table 3-15 Input and Target Data Set for ANN modeling	49
Table 3-16 Surface Roughness Predictions using different number of neurons	51
Table 3-17 Input data set for 8 runs	52
Table 3-18 Surface roughness and vibration measurements for validation runs	53
Table 3-19 Predicted Average Surface Roughness Values.....	54

Table 3-20 Repetition of 1 st run after every 5 runs	55
Table 3-21 Measurements results of one PC specimen after successive cuttings.....	55
Table 3-22 Repetition of Surface Roughness Measurement for 3 rd run	56
Table 4-1 Least Squares Means Table for feed rate.....	58
Table 4-2 Least Squares Means Table for depth of cut	60
Table 4-3 Least Squares Means Table for spindle speed.....	63
Table B-1 Technical Specifications of Pretitech Freeform 700U [21]	77
Table E-1 Technical Specifications of Zygo NewView 5000 Interferometry	83
Table G-1 Surface Roughness measurements for 27-runs testing experiment	89
Table H-1 Surface Roughness Measurements for 8-runs validation experiment.....	95

LIST OF FIGURES

FIGURES

Figure 1.1 A360 6X Night Vision Weapon Sight (Courtesy of ASELSAN) [1].....	1
Figure 1.2 FALCONEYE Electro-Optical Sensor System (Courtesy of ASELSAN)[1]	2
Figure 1.3 AVCI Helmet Integrated Cueing System (HICS) (Courtesy of ASELSAN) [1] .	2
Figure 1.4 The optical properties of a lens (adapted from [5])	4
Figure 1.5 Optical Scattering vs. Surface Roughness [8]	5
Figure 1.6 Brittle chip formation of ADC (a) and ductile chip formation of PC (b) at a cutting speed of 2.5mm/s (adapted from [13]).....	8
Figure 3.1 ANN architecture in a single hidden layer	22
Figure 3.2 Precitech Freeform 700U four-axis diamond turning machine (adapted from [21]).....	24
Figure 3.3 Four Axes of Diamond Turning Machine (adapted from [21]).....	24
Figure 3.4 Mounting of monocrystalline diamond tool	26
Figure 3.5 Tool numbering for monocrystalline diamond tool.....	26
Figure 3.6 Data Collection Setup.....	27
Figure 3.7 Mounting of the accelerometer (Top view).....	28
Figure 3.8 Mounting of the accelerometer (Front view).....	28
Figure 3.9 Numbered PC Specimens	29
Figure 3.10 Fixture for the placement of PC specimen	30
Figure 3.11 Centering of the PC specimen	31
Figure 3.12 Thickness control of the specimens.....	31
Figure 3.13 Surface characteristics and Terminology (adapted from [67]).....	32
Figure 3.14 Schematic View of Optical System of White Light Interferometry [69]	33

Figure 3.15 Zygo NewView 5000 White Light Interferometry [70]	34
Figure 3.16 Measurement points for PC specimen	35
Figure 3.17 Comparison of the measured surface roughness and predicted surface roughness of ANN model	50
Figure 4.1 Leverage plot for feed rate.....	58
Figure 4.2 The change of average surface roughness with feed rate for 27-runs testing experiment	59
Figure 4.3 The change of average surface roughness with feed rate for 8-runs validation experiment	59
Figure 4.4 Leverage plot for depth of cut	60
Figure 4.5 The change of average surface roughness with depth of cut for 27-runs experiment	61
Figure 4.6 The change of average surface roughness with spindle speed for constant feed rate and depth of cut.....	62
Figure 4.7 Leverage plot for spindle speed.....	62
Figure 4.8 Frequency response for 4 th run in 27-runs experiment	64
Figure 4.9 Frequency response for 22 th run in 27-runs experiment	64
Figure A.1 R _a Roughness Measurement [71].....	75
Figure A.2 R _q or rms Roughness Measurement [71]	76
Figure A.3 R _z or PV Roughness Measurement [71]	76
Figure C.1 Tool Numbering System for Monocrystalline Diamond Tool	79
Figure D.1 Product Data Sheet for Polycarbonate	81
Figure F.1 1 st measurement for 8 th run of 3 ^{^3} full factorial design.....	85
Figure F.2 2 nd measurement for 8 th run of 3 ^{^3} full factorial design.....	85
Figure F.3 3 rd measurement for 8 th run of 3 ^{^3} full factorial design	86
Figure F.4 4 th measurement for 8 th run of 3 ^{^3} full factorial design	86
Figure F.5 1 st measurement for 22 nd run of 3 ^{^3} full factorial design	87
Figure F.6 2 nd measurement for 22 nd run of 3 ^{^3} full factorial design	87

Figure F.7 3rd measurement for 22nd run of 3³ full factorial design 88

Figure F.8 4th measurement for 22nd run of 3³ full factorial design..... 88

LIST OF SYMBOLS

α :	Clearance angle
d:	Grating Distance
d_c :	Critical depth of cut
doc:	Depth of cut
E:	Elastic modulus
f:	Feed rate
γ :	Rake angle
γ_s :	Surface energy
h:	Depth of cut
λ :	Wavelength
PV:	Peak to valley surface roughness
r:	Tool nose radius
R_a :	Average surface roughness
R_H :	Relative Humidity
R_q :	Root mean square surface roughness
S:	Spindle speed
σ :	Standard deviation
T_g :	Glass transition temperature
TIS:	Total Integrated Scatter
Q:	Roughness sampling length
V_c :	Cutting speed

LIST OF ABBREVIATIONS

ADC:	Allyl diglycol carbonate
ANFIS:	Adaptive neuro fuzzy interference system
ANN:	Artificial neural network
ANOVA:	Analysis of variance
LM:	Levenberg-Marquardt
MCD:	Monocrystalline diamond
PC:	Polycarbonate
PS:	Polystyrene
PMMA:	Polymethyl methacrylate
SCG:	Scaled Conjugate Algorithm

CHAPTER 1

INTRODUCTION

1.1 Motivation

Optics is a main developing area of modern science and technology. Optical devices are vital components in many sectors of industry. There are many kinds of application areas such as thermal imaging systems, IR imaging systems, night vision systems, visual systems, telecommunication systems, guidance systems, medical and diagnostic instruments, projection systems, security systems, digital imaging systems and astronomical applications.

In military applications, optical systems are widely used for targeting and thermal imaging purposes. Narrow-wide field of view with superior image quality, high magnification and clear vision at long ranges can be provided by using such developed systems [1]. Some typical applications of these systems are shown in Figure 1.1 and Figure 1.2.



Figure 1.1 A360 6X Night Vision Weapon Sight (Courtesy of ASELSAN) [1]



Figure 1.2 FALCONEYE Electro-Optical Sensor System (Courtesy of ASELSAN)[1]

Lenses and mirrors are the main parts of optical devices. Functionality of these parts are crucial important to obtain better optical performance. With the developing technology, new materials have been introduced. Until the introduction of plastic lens materials in mid-1900's, glass had been the only lens material choice [2]. However, low impact resistance, high cost and heavy structure of the glasses contributed to the rise of plastics in optical applications. Also, plastics have superior advantages over other metals in terms of some properties such as corrosion resistance, electric insulation, light weight, easily and rapidly making parts in desired shapes. Polycarbonate (PC) which is a particular group of thermoplastic polymers, has been one of the best choices in optical applications because of its low weight and high impact resistance [3]. A personal system whose glasses are made from PC for attack helicopter pilots is shown in Figure 1.3. This system protects the pilot's head and face from impact and also displays video and night vision for the pilot during the mission [1].



Figure 1.3 AVCI Helmet Integrated Cueing System (HICS) (Courtesy of ASELSAN) [1]

Most of the parts used in optical systems are manufactured by injection molding. However, some custom parts such as intra-ocular lenses and spectacle lenses have to be produced according to the eye-dioptre of the customer. The current production of these lenses starts with rough cutting, then grinding and polishing processes are applied until the final optical quality is reached. However, moving parts from one process to another, unwanted pressure due to improper fixing of the parts and problems originated from the nature of grinding and polishing can deteriorate the final quality of optical parts [4]. Therefore, ultra-precision machining provides better solutions for the manufacturing of high quality parts and the minimization of problems during manufacturing process.

1.2 Surface Finish and Optical Quality

Surface finish is mainly a process to achieve a better surface from a manufactured part. However, increasing demand for very high quality surfaces makes the process a little bit complicated. Although manufacturing process produces surfaces with less than tens of nanometer accuracy, manufactured parts can still have unwanted defects. Tool marks, scratches and craters formed in material surface may cause serious problems according to application area of this material. For example; lens and mirrors used in optical systems need to have a perfect surface quality to achieve their function but tool marks and other surface defects can considerably decrease optical performance in terms of scattering and distortion [5].

Better optical properties is the one of the most important selection criteria for optical parts. Refraction, reflection, absorption, diffusion and diffraction are main optical properties and shown in Figure 1.4.

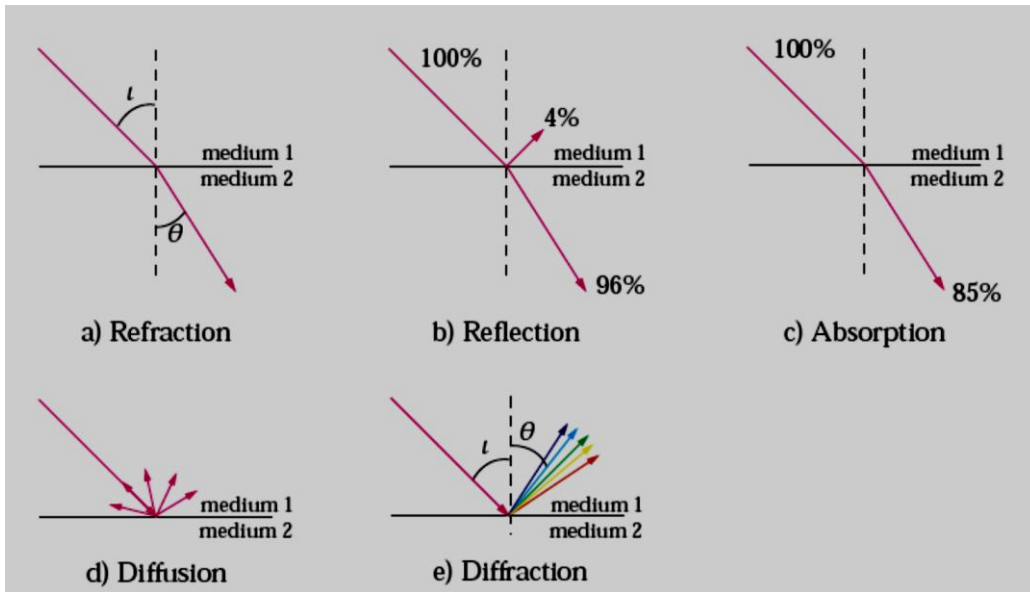


Figure 1.4 The optical properties of a lens (adapted from [5])

Refraction, reflection and absorption properties depend on material characteristics. However, diffusion and diffraction are mostly related to the manufacturing process, since diffusion is dependent on surface roughness. A scattering of a light beam at the surface is shown in Figure 1.4 (d) and a relation between diffusion and surface roughness is given by the total integrated scatter (TIS) equation [6, 7]:

$$\text{TIS} = \left(\frac{4\pi Rq}{\lambda}\right)^2 \quad \text{where} \quad (1.1)$$

TIS : the amount of scattered light with respect to the total intensity of the incident beam

Rq : the root mean square roughness of the surface (given in Appendix A)

λ : the wavelength of the incident beam

According to this equation, the larger wavelengths, the less amount of scattering but for the visual spectrum, with a shortest wavelength of nearly 300 nm, 2.4 nm Rq surface roughness is needed to have only 1% loss of intensity by scattering, hence optical parts which will be used in visual spectrum need to have better surface roughness values [5].

Figure 1.5 indicates the relation between surface roughness and optical scattering clearly where $\lambda=500\text{nm}$ and $\theta=60^\circ$ [8]. In that figure, 25nm Rq roughness is a critical value which scatters 10% of the light. According the SPI A-1 specification determined by the Society for the Plastic Industry, finished plastic molds should have R_a between 12.5-25 nm (0.5-

1 microinch). This specification is used for producing plastic mirrors, visors and other plastic goods. For optical applications, the surface could be as rough as 25nm which is equal to 35nm Rq (since R_a is about $0.7 \times R_q$). However, the surfaces should be smoother for better optical performance [8].

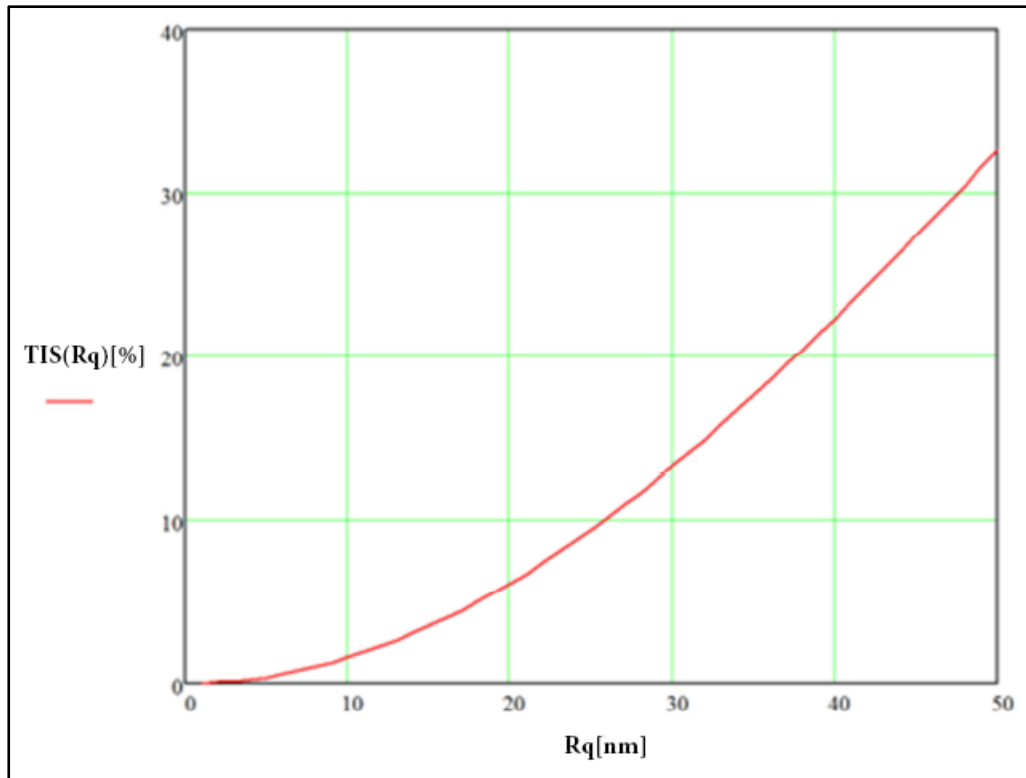


Figure 1.5 Optical Scattering vs. Surface Roughness [8]

Diffraction is also related to machining operation. In literature, it was found that there is relation between feed rate and diffraction rate by the grating equation for oblique incidence [9] as:

$$\sin \theta = \sin \tau + \frac{m\lambda}{d} \quad \text{where} \quad (1.2)$$

m : the order of the interference line

λ : the wavelength of the used light

d : the grating distance

ι : the angle between surface normal and incident light beam

θ : the angle between surface normal and diffracted light beam

A rainbow image at the surface of diamond turned optical parts is caused by a white light ray incidents on a surface with regularly spaced pattern. Guido [5] stated that if the feed rate f is constant, d equals to f and amount of diffraction can be calculated by Equation (1.2). From this equation, it can be understood that if the feed rate is less than wavelength of the used light, there will be no diffraction which will result in low production rate.

1.3 Machining of Plastics and Polycarbonate

Plastics are widely used in terms of weight and economic considerations. Their low price and low specific gravity makes plastics very attractive for all industrial applications. However, despite the demand for plastics having high level of surface quality and accuracy are so high, micro-machining of plastics is not very popular.

Although most of the plastics are manufactured by various molding processes such as injection molding, extrusion or compression molding, manufacturing of parts which are intricately and precisely shaped are essential [10]. Same traditional methods and cutting tools to machine metals are mostly being used for plastic machining. However, manufacturing process of plastics differs from the metal cutting process in some aspects.

Cutting temperature of plastics during machining is not as high as that of metals but the rate of tool wear and the final surface quality is directly affected by cutting zone temperature in the machining of plastics [machining and surface integrity of polymeric materials]. If the glass transition temperature of plastic is reached, a better quality surface finish is achieved and the material removal process will be in ductile manner. That increase in temperature causes a decrease in shear stress and tensile strength due to rapid movement of molecular chains of plastic [11].

Estimated temperature rise of some plastics experimented by Smith [12] is illustrated in Table 1-1. Thermal flow temperature of these polymers (Glass transition temperature for Polystyrene (PS), Polycarbonate (PC) and Polymethyl Methacrylate (PMMA): 100°C, 150°C and 165°C, respectively) are well above the temperatures in Table 1-1. Therefore, a

thermal viscous flow during machining is not expected.

Table 1-1 Estimated temperature rise by Smith [12]

Smith's set	v _c (m/s)	R (mm)	f (μm/rev)	h (μm)	Temperature rise in		
					PS	PMMA	PC
1	0.3	3.175	50.80	12.7	59K	50K	70K
	1.5	3.175	50.80	12.7	91K	88K	92K
2	0.3	0.762	50.80	12.7	64K	64K	65K
	1.5	0.762	50.80	12.7	97K	97K	103K
3	0.4	0.762	10.16	12.7	42K	25K	23K
	4.0	0.762	10.16	12.7	88K	85K	87K
	10.0	0.762	10.16	12.7	96K	100K	105K
4	0.4	0.762	3.81	12.7	7K	5K	1K
	4.0	0.762	3.81	12.7	73K	66K	68K
	10.0	0.762	3.81	12.7	91K	90K	94K

Chip formation process is also known as an important phenomenon. Ductile and brittle modes of machining affect the surface quality to a large extent. An experimental study was conducted to show the chip formation in polymer cutting. Different chip structures from thermosetting ADC and thermoplastic PC were shown in Figure 1.6. It can be easily seen that crack propagation of below the depth of cut causes a bad quality surface, on the other hand, ductile chip formation results in good surface quality as seen in PC experiment [5].

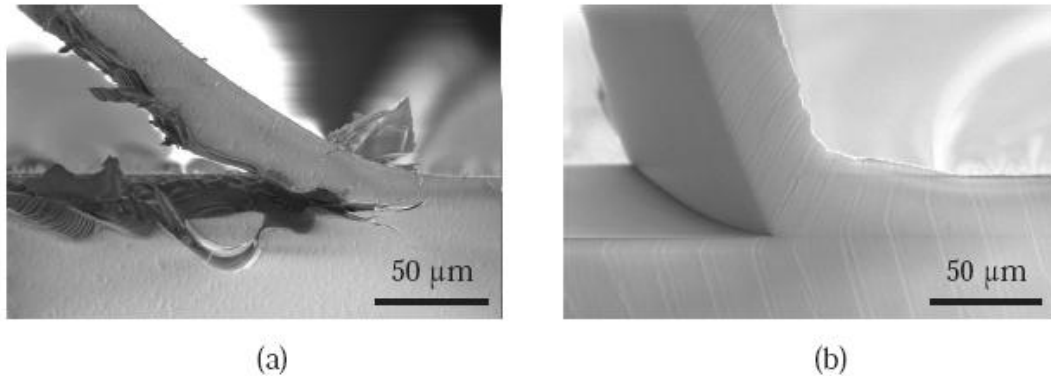


Figure 1.6 Brittle chip formation of ADC (a) and ductile chip formation of PC (b) at a cutting speed of 2.5mm/s (adapted from [13])

Tool wear is another phenomenon during plastic machining. Contrary to common belief, diamond tool wear during plastic machining can have hazardous effect on final quality of plastic parts. Electrostatic charging between diamond tool and polymer causes luminescence effect on the tool surface and the cutting edge of the tool is damaged. Increasing relative humidity (RH) above 70% can help preventing charging effect which is experimented by industry. Experimental studies also showed that tool wear is more possible during cutting polymers which has a higher chain density. The use of water as cutting mist and spray can be another solution for electrostatic charging [14]. However, experimental studies conducted in humid conditions did not considerably reduce the wear of tool during machining PC which shows that there can be another mechanism of tool wear.

1.4 Aim and Scope of Thesis

Optical systems is a rapidly developing area in military applications. There is an increasing demand for plastic parts to use in optical industry due to their lower weight and higher impact resistance. There are several different production techniques to produce optical parts. Single point diamond turning is one of the most popular techniques to manufacture complex and low volume production parts. However, single point diamond turning is a non-linear process which depends on many parameters such as tool geometry, tool-workpiece interaction, cutting parameters, machine vibration and material properties etc. Because of these complex relations, the prediction of surface roughness for diamond-turned parts is really difficult. Since surface roughness values of the machined surface has great

importance, the optimization of cutting parameters is main concern in this study.

There have been many studies about the optimum machining conditions for a good surface quality however only few of them have achieved really high quality surfaces for plastic machining.

This study focuses on machining of polycarbonate to obtain the best optical quality. On the basis of recent studies in literature and the recommendations of tool manufacturers, tool parameters like rake angle, clearance angle and tool nose radius were taken as 0° , 10° and 0.5 mm, respectively. The effect of feed rate, depth of cut and spindle speed on surface roughness were analyzed and vibration data taken from tool holder during machining process were used to find a correlation between tool vibration and surface roughness of polycarbonate specimens. Peak to Valley (PV), average surface roughness (R_a) and root mean square (R_q) values of PC specimens were measured by Zygo NewView 5000 White Light Interferometry. Three-level full factorial design, artificial neural network modeling and statistical methods will be implemented to correlate the surface roughness with tool vibration and cutting parameters.

CHAPTER 2

LITERATURE SURVEY

2.1 Introduction

Single Point Diamond Turning is a ultra-precision machining process that is widely used to produce high-quality optical elements from metals and plastics. Diamond turning has always been an important machining process throughout the history. In 1901, Carl Zeiss Company used single point diamond turning to produce aspheric surfaces but the quality was not good enough to use in camera lenses [15, 16]. In 1929, lenses having high accuracy level surface finish could be manufactured by Bausch [17]. Later, Taylor and Robson [18] developed a polar coordinate aspheric generation machine to produce high quality camera lenses.

Despite advances in the ultra-precision turning, it is not always easy to achieve a high quality surface finish. Lots of parameters such as machine tools, cutting tools, work-piece material and machining process affect surface quality during turning. Too many investigation has been made to optimize parameters to have a better surface finish.

Since polymeric materials were started to use in optical applications, diamond turning of plastics have been studied profoundly. Several researches have been made about cutting behavior of plastic materials. Smith[12] made a study about the relationship between the glass transition temperature of the polymer and the surface roughness and claimed that ductile chip is formed due to adiabatic heating with the increasing cutting speed. The details of this study is given in Section 2.4. Guido investigated that hypothesis after turning polymers (PS, PMMA and PC) with different cutting conditions. He found that glass transition temperature is not reached in diamond turning of investigated polymers. He showed that there can be little temperature increase in primary shear zone when cutting speed increases but it is not enough to reach glass transition temperature in PC. Guido also studied about the wear mechanisms during turning plastics and they found that both tribo-electric and tribo-chemical wear significantly affect tool wear during turning polymers [5].

Saini et al. [19] made a research about determining optimum parameters for a better surface finish during turning PC. They changed several parameters to achieve high surface quality.

They suggested that 0.5 $\mu\text{m}/\text{rev}$ feed rate, 2 μm depth of cut and 3000 rpm gives best results during turning and 25.4 nm average surface roughness is achieved with an old diamond tool.

Carr and Feger [20] made a study about the material removal mechanisms during diamond turning of polymers and revealed that material and visco-elastic properties play an important role to achieve a better surface quality. They also stated that every specific material need to be analyzed to have a better understanding about diamond turning of polymers.

In 2010, Yergök [21] made an experimental study about single point diamond turning of germanium. In his study, he tried to optimize cutting parameters such as rake angle, depth of cut, feed rate and cutting speed by using “Box Behnken” and “Full Factorial” design methods.

2.2 Wear Mechanisms During Cutting Plastics

Tool wear is a serious problem which affects machining ability. It causes both economic problems and quality problems during machining. Contrary to the belief that there is not much tool wear during diamond turning of polymers, considerably large tool wear has been observed during experiments [14, 22].

In literature, tool wear during cutting plastics haven't been much studied but nevertheless there are quite enough resources to identify wear mechanisms on tool wear. Evan [23] classified tool wear into four main categories such as adhesion, abrasion, tribo-thermal and tribo-chemical but Guido [5] added one more wear mechanism called tribo-electric tool wear during discharging effects during lens production. Since diamond tool and glassy polymers are insulators, there can be friction due to static electricity between tool and work-piece. However, tribo-electric tool wear mechanism was not dominant for the used polymers. According to their study, tribo-chemical tool wear plays important role during cutting PC and PMMA since they observed chain scission which causes highly reactive radicals during cutting PC and PMMA. That research also contradicts with the work of Paul and Evans who claimed that no chemical tool wear is occurred during turning plastics since they don't have unpaired d-electrons [24]. Guido et al. [22] also concluded their study by making emphasis on that more than one tool wear mechanism can play important role at the same time during turning plastics.

Wada et al. [25] analyzed the effect of tool wear on surface roughness during cutting of nylon and they observed wear pattern under a scanning electron microscope. They studied how homogeneity of the material and tool shape affect the wear process and observed two

kind of wear mechanism such as frictional wear and fracture wear due to cleavage.

Measurement of diamond tool wear also plays important role in diamond turning process because the severity of tool wear determines tool replacement time. There are different methods such as SEM (scanning electron microscopy), AFM (atomic force microscopy) and EBID (electron-beam-induced deposition) to measure tool wear [26]. High resolution image of tool edge sharpness can be viewed by SEM. Acoustic emission and noise measurement has also been used to detect tool wear and some correlation has been found a correlation between the sound emitted during machining and cutting tool wear rate [27].

2.3 Effect of Material Characteristics on Surface Roughness

Experiment results indicate that the quality of a diamond turned surface is determined by both the process factors including feed rate, spindle speed, depth of cut in addition to relative tool-work-piece vibration due to machine vibration and material factors such as material anisotropy, swelling and crystallographic orientation of work materials [28]. Different characteristics of materials may affect the cutting process drastically. Tensile strength, degree of crystallization and molecular weight are also effective properties which may determine the accuracy level of machining process [29].

Lee et al.[30] notified that the variation of the crystallographic orientation of the work-piece material can induce such a vibration that can cause an important change in the surface modulation frequency formed in machined surface.

Carr and Feger [20] studied about the effect of molecular weight on surface roughness. They showed that increasing molecular weight causes higher surface roughness for different PMMA grades and based on that information, they concluded that cutting of polymers occurs in the thermal flow regime.

Guido indicated that crosslink density is not a distinctive parameter to determine the surface roughness as opposed to what Carr and Feger [20] mentioned that crosslinked materials cannot be turned to a high optical quality because of their brittle behavior. Guido experimented different PMMA grades with changing crosslink density and stated that PMMA grades with higher cross linked density still had optical quality and low R_a value [5].

Zhang and Xiao [31] also mentioned that viscous deformation of a polymer plays an important role to obtain a better surface quality and they also mentioned that glass transition temperature, fracture toughness and molecular mobility are the most important polymer properties for an optimal machining condition.

2.4 Effect of Temperature on Surface Roughness

In this section, the effect cutting temperature in determining the surface quality and tool life will be explained. Although there have been few studies about the relationship between cutting temperature and surface roughness, temperature increase during diamond turning may play an important role to determine the final surface quality. Since, increasing temperature in the cutting zone may result in significant tool wear and the change in deformation characteristics of materials which will be diamond turned [32].

Smith [12] stated that more thermal softening is a result of an increase in cutting speed and better surface quality is expected when the polymer reached a thermal softening point. However, Guido [5], with regard to his thermal model, argued that increase in cutting speed is not very effective for a significant additional temperature increase in the primary shear zone. Besides, in his study, it is stated that with the increasing cutting speed most of the generated heat during cutting action is transported to chip via heat conduction and material transport.

Lubricants also determine the efficiency of machining operations due to their lubrication, cooling properties. Kamruzzaman et al. declared that the use of high-pressure coolant resulted in significant decrease in tool wear, surface roughness, cutting forces and significant increase in tool life by means of temperature decrease and the change in tool-work and tool-chip interaction [33].

Wang et al. also stated that oil-air lubrication is much more effective in reducing the cutting temperature than wet and dry cutting and also helps avoiding environmental pollution and reducing running and maintenance costs [34].

Herbert [35] experimented chip-tool interface temperature change under different cutting conditions by using a tool-work thermocouple system. He analyzed the temperature increase with the varying cutting speed and different cutting fluids. He revealed that temperatures increase with the increasing speed from 0.1 m/s to 1 m/s and when he compared the results after dry cutting, cutting with oil lubricant and cutting using just water as the cutting fluid. Cutting with water gave the best results due to the fact that water is the best heat conductor among the others. However, water causes some serious problems such as corrosion on the machine tool and work-piece and insufficient lubrication.

2.5 Effect of Vibration on Surface Roughness

In the manufacturing industry, vibration is always an important parameter which affects the cutting process. Machining vibration is influenced by different sources such as structure of machine, type of tool, work material, etc. Forced and self-excited vibrations are known as the main types of the machining vibration. Unbalanced machine-tool components, misalignment, bad gear drives are the main reasons for force vibration. Self-excited vibration is generated from the interaction of the chip-removal process and the machine-tool structure which deteriorates the surface quality of the machined surface [36, 37].

Asiltürk [38] analyzed the effect of depth of cut, feed rate, nose radius, cutting speed and vibration on the surface roughness of AISI 1040 steel. He developed an ANFIS predictive model based on vibration monitoring but in that study, vibration effect was not taken in three axes instead used as general mean vibration amplitude. Sohn et al. [39] claimed that vibration is second important factor behind feed rate assuming good tool edge quality and proper material selection. In their study, they indicated that gradually decreasing feed rate is not a reasonable way to have a good surface roughness because after some point, environmental and material effects dominate the machining operation and lower feed rates than $2\mu\text{m}$ using a 0.5 mm radius tool do not enhance the surface quality.

Abuthakeer et al. [40] studied the self-excited vibration analysis of the spindle bearing. In their study, they investigated the natural frequency and vibration response of the system with the varying parameters such as feed rate, depth of cut and cutting speed. Accelerometers were used for sensing vibration due to their practical use and capability of measuring deformations and forced vibrations compared to microphones.

In the study of Lee et al. [41], material induced vibrations were underlined due to the fact that depth of cut is very small, in order of micrometer, in diamond turning and that is smaller than the grain size which makes cutting process perform in a single grain. Therefore, the quality of the machined surface is greatly influenced by the change of material microstructure.

Chen and Chiang [42] used the rubber-layered laminates to reduce the vibration amplitude in tool-tip in diamond turning of Al6061-T6 aluminum alloy. They experimented styrene and butadiene rubber (SBR) and silicone rubber (SI) as rubber materials. They found 5.77% and 13.22% better surface roughness values by using SBR and SI, respectively. The best surface roughness achieved in that experiment was $0.13\mu\text{m}$.

Baek et al. [43] indicated that the relative displacement of the tool in cutting direction is not very effective in the surface generation and the surface roughness in the infeed cutting direction is more dominant.

Kassab and Khoshnaw [44] studied the effect of cutting tool vibration on surface roughness of workpiece. They concluded that cutting tool acceleration has an important effect on surface roughness and the effect of cutting tool vibration in feed direction is very smaller than that in the vertical direction. It was found that vibration in a single direction, as well as the main cutting parameters such feed rate, depth of cut, and spindle speed can be used for predicting surface roughness. However, Armarego et al. [45] showed that vibration in all direction exists in a cutting process and surface roughness can be influenced by vibration in each direction. In Dimla's study [46], vibration features are used to monitor tool-wear procedure in a metal turning process and the procedure showed that wear qualification of cutting tool is influenced by the vibration signals.

2.6 Optimization of Parameters Affecting Surface Roughness

Due to the increasing demand for better surface finish and dimensional accuracy, machining process requires the optimal use of cutting parameters, measuring techniques and experimental design methods. Final surface quality of a workpiece in a ultra-precision machining process can change depending on tool parameters (nose radius, rake angle, clearance angle), cutting parameters (feed rate, depth of cut, cutting speed) and all other process parameters such as coolant, tool-workpiece interaction, machine vibration. Optimization of parameters in manufacturing is not very easy to achieve due to nonlinear structure of the machining process. There are so many variables which can affect the process significantly. However, the main purpose is to obtain a low surface roughness and less tool wear in terms of production rate, operational cost and quality of machining[19].

Experimental design methods, statistical methods and mathematical models have been used to analyze the results of the experiments. Thus, empirical relations have been found to relate the surface roughness with the cutting variables. In literature, many studies have been conducted to optimize surface roughness by varying machining parameters and by implementing different experimental methods. Özel and Karpaz [47] investigated the effect of depth of cut, feed rate and insert radius on surface roughness in turning of AISI 1030 steel bars by using Taguchi method. Çalı [48] studied the effect of cutting parameters and rake angle during single point diamond turning of silicon. 2^3 factorial design method used to optimize parameters and best average surface roughness achieved is 1 nm. In the study of Aslan et al. [49], an orthogonal array and analysis of variance method had been used to optimize the cutting parameters such as cutting speed, feed rate and depth of cut and final surface roughness of turned AISI4140 steel and flank wear of Al_2O_3 ceramic tool coated with TiCN were examined as quality objectives. Al-Ahmari [50] used response surface methodology and neural networks to compare and evaluate the relationship between cutting parameters and surface roughness by developing empirical models on turning of austenitic

AISI 302. Kopac et al. [51] studied the effect of cutting speed and feed rate variations on recorded noise amplitude and found that as compared to feed rate, cutting speed does not have too much effect on sound vibration. Huang and Chen [52] developed a multiple regression model to predict the in-process surface roughness of Aluminum 6061T2 in a turning operation by using feed rate, depth of cut and spindle speed and vibration which is obtained via an accelerometer on tool holder as predictors. They obtained 1.55% greater accuracy level in predicting surface roughness by using vibration information than that of the model which has no vibration information. Xu et al. [53] conducted another experimental study about the diamond turning of silicon, germanium and aluminum alloy (Al 6061). Moore Nanotech 250UPL lathe and Newview 7300 interferometer were used for that experiment. 0° rake angle for aluminum and -25° rake angle for germanium and silicon had been chosen due to different machining characteristics of materials. The best average and rms surface roughness value measured for aluminum was 1.6 nm and 1.2 nm, respectively. For silicon, best values were 0.46 nm rms surface roughness and 0.37 nm average surface roughness. As for germanium, 0.58 nm rms surface roughness and 0.42 nm average surface roughness values were the best. Khatri et al. [54] studied the effect of machining parameters on surface roughness during diamond turning of polycarbonates. They also tried to find out the profile error to optimize tool path. During experiments, the best achieved average surface roughness value was about 50 nm. Singh et al. [55] also observed the surface roughness and waviness during machining of polycarbonate. They concluded that surface roughness and waviness are increasing with machining time. 9 nm surface roughness was the best achieved surface roughness during their experiments. Guido[5] also investigated different polymeric materials and machined polymers in different cutting conditions. However, the optical quality of polycarbonate could not go under the accuracy level of 10 nm average surface roughness.

In literature, there are few experimental studies about the diamond turning of polycarbonates as stated above. In Table 2-1, the best achieved average surface roughness values and process parameters are given.

Table 2-1 The best achieved surface roughness values during the diamond turning of polycarbonate in literature

Reference Citation	v_c (m/s)	f ($\mu\text{m}/\text{rev}$)	doc (μm)	S (rpm)	γ	α	r (mm)	R_a (nm)
Guido, 2006[5]	0.3	-	10	-	3.6°	15°	1	10
Guido, 2006[5]	3	-	10	-	0°	15°	1	11
Khatri et al. 2012[54]	-	1	2	2000	0°	10°	1	50
Saini et al. 2012[19]	-	0.5	2	3000	0°	10°	0.5	25.4
Singh et al. 2013[55]	-	1	15	2000	0°	10°	0.5	9

CHAPTER 3

DESIGN OF EXPERIMENTS, EXPERIMENT PROCEDURE AND RESULTS

3.1 Introduction

In this chapter, main components used for diamond turning of polycarbonate for optical applications will be clarified. Firstly, experimental design methods will be introduced to find a correlation between surface roughness and process parameters. Comparisons among these methods will be figured out. Then, a brief description of single point diamond turning setup will be made. Later, main characteristics of diamond tool setup and vibration data collection system will be introduced. Lastly, the preparation of workpiece setup will be mentioned and surface roughness measurement methods will be clarified.

3.2 Experimental Design

In this thesis study, main objective is to machine polycarbonate to optical quality and predict the surface roughness for saving cost and time for high production rates. Therefore, most important factors in this machining process need to be highlighted. Different experimental methods are used to analyze the effect of main parameters and predict the surface roughness during cutting process. As mentioned in Chapter 2, there are different strategies which are the fuzzy set-based approach [38], multiple regression techniques [52], artificial neural network approach [50] and full factorial design [48] to analyze the machining process. Full factorial designs and artificial neural network (ANN) have some advantages over other methods. Full factorial designs can reduce the number of runs significantly and provide useful information about the process parameters. As for artificial neural network approach is very effective if there is too much parameters to control. Complex relationships between input and output parameters can be modeled accurately and

reliable and robust models can be obtained. Due to their advantages, three level full factorial design and artificial neural network approach will be used in this experimental study.

3.2.1 Three Level Full Factorial Design

Design of the experiments (DOE) is a mathematical methodology to determine the most relevant factors in a process and provide interpretation of the results and also predict the possible results for high accuracy. It gives very producible results by minimizing the number of runs with the minimum cost [56].

DOE starts with determining the objectives of the experiment and choosing the factors to be investigated. Experimental designs have three main objectives: Comparative, Screening and Response Surface. Comparative objective is used to identify one important factor and its effect on changing response excluding other parameters. Screening objective is used to eliminate the many less important effects during experiment. It focuses for identifying the main important factors affecting response. Response Surface Objective is mainly used to optimize the response and make the process more robust [57]. Main design of experiment methods are given in Table 3-1.

Table 3-1 Design of Experiments Methods [58]

Number of Factors	Comparative Objective	Screening Objective	Response Surface Objective
1	1 Factor Completely Randomized Design	–	–
2 to 4	Randomized Block Design	Full or Fractional Factorial	Central Composite or Box-Behnken
5 or more	Randomized Block Design	Fractional Factorial or Plackett-Burman	Screen First to Reduce Number of Factors

In this study, three-level full factorial design which is one of the screening objective design of experiment methods is performed on flat surface by considering three parameters as spindle speed, depth of cut and feed rate. The advantage of implementing three-level factorial design is to reduce the number of runs and study all paired interactions with three factors. In three-level full factorial design, the highest, the lowest and the middle points of these parameter values are used and thus 27 runs are performed. The highest values are represented by (+1), the lowest values represented by (-1) and the middle points of these values are represented by (0). Performed runs are tabulated in Table 3-2.

Table 3-2 Runs for Three-level Full Factorial Design with Three Parameters

Run	Parameters			Run	Parameters		
	A	B	C		A	B	C
1	0	+1	+1	15	0	+1	-1
2	+1	0	-1	16	0	-1	-1
3	0	0	+1	17	+1	-1	-1
4	+1	0	+1	18	-1	0	-1
5	+1	-1	0	19	-1	-1	-1
6	0	-1	+1	20	0	0	0
7	-1	+1	-1	21	0	+1	0
8	-1	-1	+1	22	+1	+1	+1
9	-1	+1	+1	23	+1	+1	-1
10	0	-1	0	24	-1	0	0
11	-1	0	+1	25	+1	+1	0
12	-1	+1	0	26	+1	-1	+1
13	0	0	-1	27	+1	0	0
14	-1	-1	0				

Finally, the relation between surface roughness of machined polycarbonate and cutting parameters like spindle speed, depth of cut and feed rate is determined by using mathematical models which is obtained from DOE methods. Finally, an analysis of variance (ANOVA) is performed using JMP to explore the significance level of parameters on surface roughness of polycarbonate. All results from experimental methods and all data collected from ANOVA studies will be given in Chapter 3.

3.2.2 Artificial Neural Network Approach

With the developments in computer technology, ANN has been very effective method to study nonlinear systems with a large number of variables. It provides fast and reliable results for complex systems with less experimental data [59].

The main element of ANN is a neuron whose shape and size can change according to its function. A neural network contains the input layer neurons, hidden layer neurons, and an output layer. A simple presentation of ANN is shown in Figure 3.1.

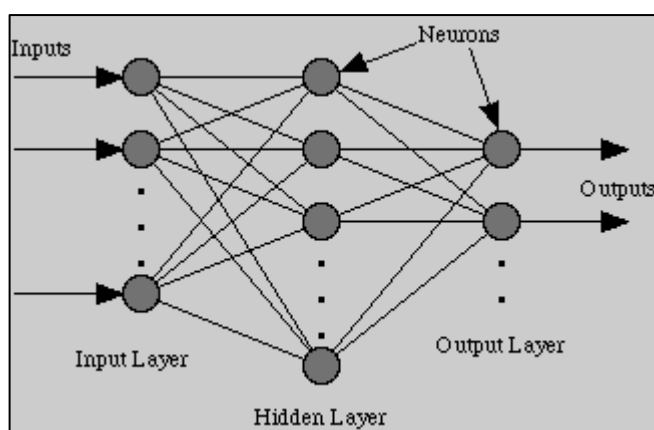


Figure 3.1 ANN architecture in a single hidden layer

Combination of neurons with different weighted interconnections constructs the neural networks. In ANN approach, an algorithm such as Levenberg-Marquardt (LM) back propagation or scaled conjugate gradient (SCG) back propagation is used to determine these weights. ANN maps between input and output data sets. For mapping, training is the most important duty. Input and output data is defined for the network and ANN starts training with these parameters. ANN continues learning the system during the training. Learning procedure may change according to given data to the network. ANN trains the input data and tries to minimize the error by comparing the prediction values with the actual output data. Since the number of neurons in the input and output layers are known, the number of hidden layer neurons determine the efficiency of the network. Limited number of neurons can decrease the learning performance, while too many hidden layer neurons can causes the reduction in learning speed and sometimes stop the learning completely. Therefore, trial and error method is used to optimize the process[60].

In the thesis, Matlab 7.9.0 Neural network toolbox with a two-layer feed-forward network with sigmoid hidden neurons and linear output neurons is used to predict surface roughness. The same data set which is prepared for three level full factorial design is used as input data set of the ANN. Additionally, V_x (vibration in x direction), V_y (vibration in y direction), and V_z (vibration in z direction) is added to the network. Thus, feed rate, depth of cut, spindle speed, V_x , V_y and V_z are used as input layer parameters. The surface roughness will be used as output layer of the ANN. A single hidden layer of different number of neurons is implemented. The behaviors of networks with varying number of neurons are tabulated in Chapter 4. The prediction values for training data and test data which has never been trained before, are also tabulated and compared in Chapter 4. Finally, an independent sample t test was carried out to show reliability and applicability of ANN by using IBM SPSS Statistics 20 software.

3.3 Single Point Diamond Turning

Single Point Diamond Turning is a ultra-precision machining process for producing high quality optical surfaces on metal, polymers and crystals. In diamond turning, work piece is pulled onto a vacuum chuck, whose surface quality is within a few fringes, the spindle rotates with high precision with the help of air bearings, the tool is numerically controlled and a laser interferometer monitors its movements. A submicron level dimensional accuracy and nanometer level surface roughness can be achieved by diamond turning with a single point cutting tool. In addition to optical materials, materials such as magnesium, aluminum, gold, beryllium, nickel, tin, and copper are compatible with diamond turning [61].

Surface quality can be affected by so many factors such as vibration, change in humidity and partial pressure of atmospheric gases and temperature during ultra-precision machining with diamond turning. To minimize negative effects of vibration, balanced air bearing spindles, closed loop controllers using laser interferometric feedback, mounting the machine on a block of granite with vibration isolation material can be used. Temperature control is also very important to maintain good surface quality and preventing machining errors, therefore the work piece, machine and its components should be in thermal equilibrium before material removal starts. Surface finish is also affected by machining parameters such as the radius of cutting tool, feed rate, depth of cut, spindle speed, rake angle, tool wear, coolant fluids, the material being machined [62].

In this study, Precitech Freeform 700U four-axis diamond turning machine is used as shown on Figure 3.2 and the specifications of the machine are given in Appendix B. The four axes of the machine are shown on Figure 3.3. Control of only two axes (X and Z) are sufficient for machining of flat, spherical, aspheric or diffractive optical surfaces.



Figure 3.2 Precitech Freeform 700U four-axis diamond turning machine (adapted from [21])

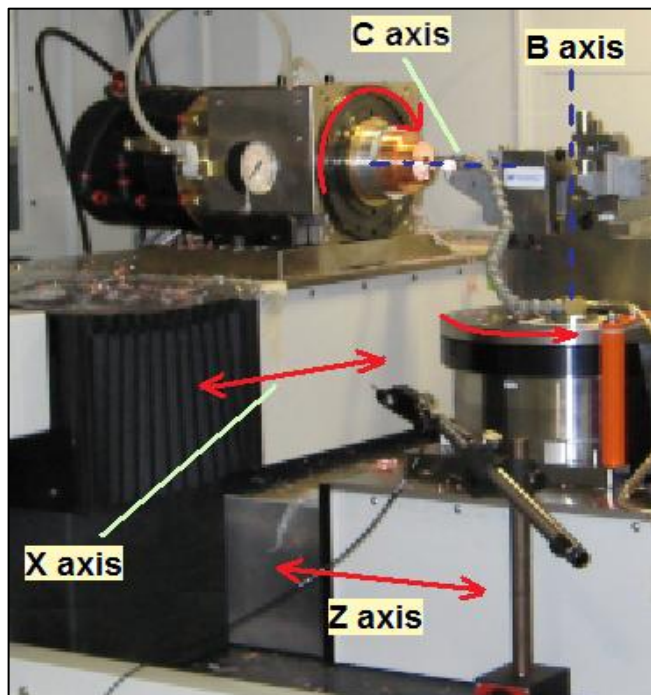


Figure 3.3 Four Axes of Diamond Turning Machine (adapted from [21])

3.4 Mono-crystalline Diamond Tool Setup

In advanced machining, the selection of cutting tool is very important. Final surface quality is affected by several error sources such as tool setting, environmental conditions, fixturing, and tool waviness. However, controlled waviness tools can decrease such kind of errors and production costs can also be decreased by choosing appropriate tools. In controlled waviness tools, the radius shape deviates from a true circle by a certain value and even less than 50 nm deviation can be reached [63].

As mentioned in Section 2.1 and Section 2.6, tool parameters can also affect the final surface roughness of machined parts. Therefore, suitable tool parameters are chosen according to experiments in literature and manufacturer's suggestions.

In this study, mono-crystalline controlled waviness diamond tool is used to machine PC specimens. In manufacturer's catalog, the suggested rake angle is between $+2.5^\circ$ and -2.5° and the clearance angle is between 5° and 15° . Tool rake and clearance angles are chosen as 0° and 10° , respectively throughout the experiment.

The monocrystalline diamond tool is mounted on a tool holder (Figure 3.4) by means of M5 screws. The tool numbering system for diamond tool is given in Appendix C and a sample tool number on the tool is shown in Figure 3.5.

According to the tool numbering system of manufacturer, the tool has following properties;

- C: Controlled waviness tool
- 0.5m: Tool has 0.5 mm radius
- L: 0° rake angle
- G: 10° front clearance angle



Figure 3.4 Mounting of monocrystalline diamond tool



Figure 3.5 Tool numbering for monocrystalline diamond tool

3.5 Vibration Data Collection Setup

A vibration data collection system (Figure 3.6) is established to determine a relation between tool vibrations and surface roughness of the final product.

The vibration data collection system includes an accelerometer (Bruel & Kjaer 4524B) from which signals are amplified, an analyzer (Pulse Front End 3560C) which obtains data from the accelerometer and a software (Pulse 16.0) which is processing all input data. Data collection setup is shown in Figure 3.6.



Figure 3.6 Data Collection Setup

The accelerometer is mounted onto lateral face of tool holder as shown in Figure 3.7 and in Figure 3.8. Same axes notation were used between the accelerometer and the lathe.



Figure 3.7 Mounting of the accelerometer (Top view)



Figure 3.8 Mounting of the accelerometer (Front view)

3.6 Work-piece Setup

Before implementing this experiment, first of all solid polycarbonate sheet called Makrolon® UV is purchased from the Sancaksan company. This company brings all PC products from Bayer Makrolon Sheet Europe company. The product data sheet of the PC is given in Appendix D [64]. The PC sheet was 2050 mm long and 1250 mm wide and 10 mm thickness. Then, this Makrolon sheet is cut into 50 specimens whose diameters are 30 mm by using Hermle C40 Machining Center (5 axes) [65]. All specimens are numbered as shown in Figure 3.9.



Figure 3.9 Numbered PC Specimens

After preparing the specimens, a fixture which has a 30 mm inside diameter is produced to place PC specimens as shown in Figure 3.10. This fixture is machined from Ertalyte® material which is not easily affected from temperature changes.



Figure 3.10 Fixture for the placement of PC specimen

Since the alignment of the axis of work piece with the axis of the spindle is critical to obtain high quality optical surfaces, PC specimen is centered by using a dial indicator which is controlled by the turning machine. After placing PC specimen into the vacuum chuck by using negative air pressure, the probe of the indicator is touched on the lateral face of workpiece and then machine operator revolves the chuck slowly by hand and report all deviations on the dial. According to the manufacturer's catalog, concentricity difference of axes needs to be less than $0.5 \mu\text{m}$ for finish operations. This process was repeated until reaching below that value and the same centering operation is applied for every run. The adjustment of the workpiece is shown in Figure 3.11.



Figure 3.11 Centering of the PC specimen

When the thickness of all of the specimens are measured by touching the probe of thickness gage to the specimen upper surface as shown in Figure 3.12, considerable differences are observed between thicknesses so all specimens are turned to the same thicknesses.

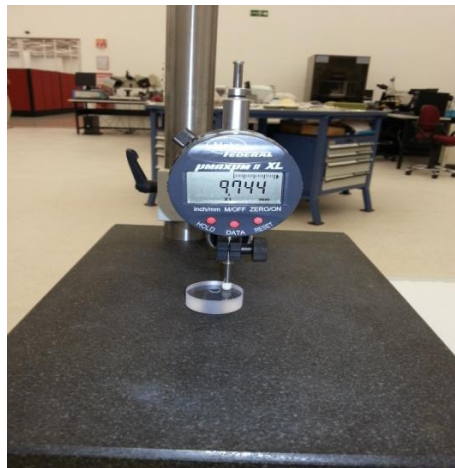


Figure 3.12 Thickness control of the specimens

After completing tool and work piece setup, the cutting parameters for each run are entered to machine program and all runs are completed.

3.7 Surface Roughness Measurement

Surface roughness plays a critical role in determining the optical performance of many devices. The amount of light scattering at the intended wavelength of operation is a major parameter for optical performance because rough surfaces scatter light which is undesirable for optical systems. Scattering needs to be controlled by limiting the surface roughness [8]. Therefore, it is very important to measure and analyze the surface texture.

The surface texture comprises two components: waviness and roughness. The roughness represents the more closely spaced peaks and valleys and usually produced by the surface forming processes. The waviness consists of the more widely spaced irregularities due to vibration in machining process. The surface topography also includes other irregularities such as form error. The lay is used to indicate the direction of dominant pattern of texture on the surface and the lay pattern formed by machining processes is generally strong and unidirectional [66]. Figure 3.13 shows the main components of the surface topography.

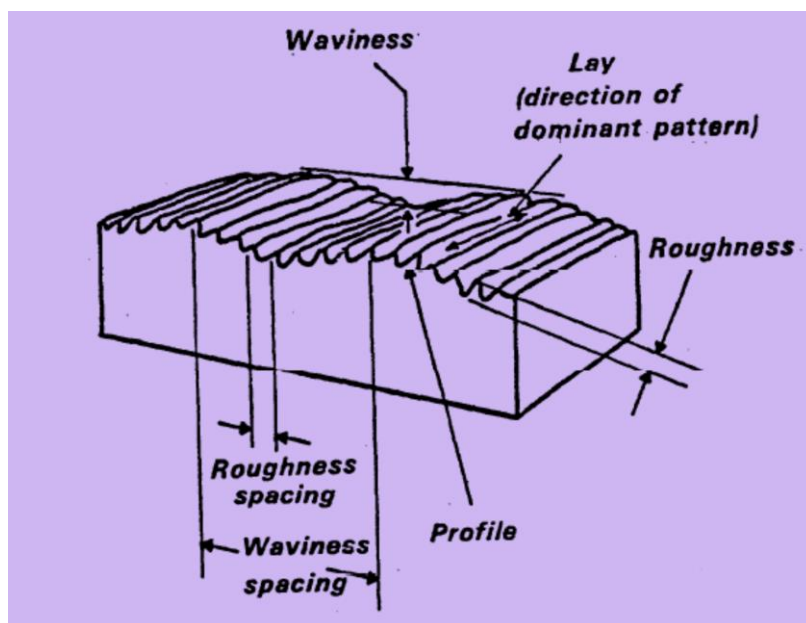


Figure 3.13 Surface characteristics and Terminology (adapted from [67])

During the machining, it is inevitable to have some defects and impurities on the surface of the machined parts. Work piece material properties, machine vibrations, surface damage due to chip formation and inaccuracy of spindle and tool holder can cause such defects on the surface and surface roughness is the result of all these irregularities [68]. There are numerous methods to measure surface roughness. They are mainly divided into two types: contact methods and non-contact methods. Stylus instruments like a simple touching probe, using a contact measurement method, have limited flexibility for measuring surface roughness of different parts due to low measurement speed and limited contacting ability to the precision surfaces. General principle is that the stylus transverses the peak and valleys on the surface and the transducer converts the vertical motion of the stylus to the electrical signal. Finally this signal can be analyzed by analogue or digital techniques and it can be stored in computer to be analyzed for roughness and waviness parameters [67].

However, optical and computer vision methods such as laser scanning confocal microscopy and white light interferometry are much more useful for 3D characterization of different surfaces. In white light interferometry method, a beam splitter separates the light and while one beam is pointed to the referenced surface, the other beam is guided to measured surface. Then, these beams are reflected from the surfaces and they interfere with each other inside the optical system. Finally, the light and dark fringe pattern produced by these interferences produces the 3D interferogram of the surface which will be transformed to 3D image structure with surface profiles [69]. A schematic showing how scanning white light interferometry working is illustrated in Figure 3.14.

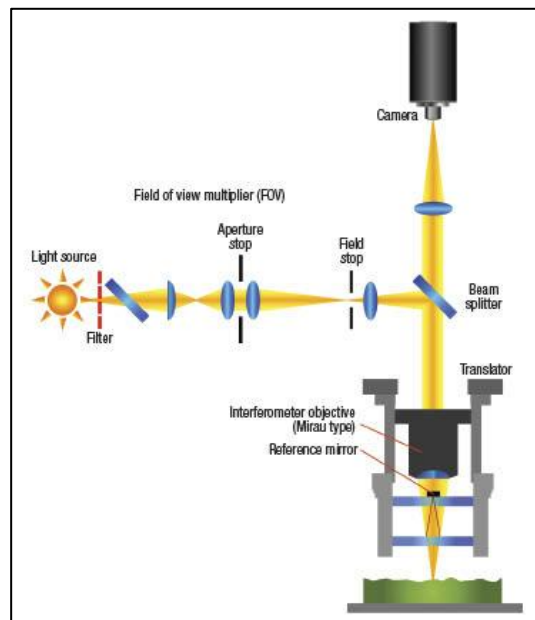


Figure 3.14 Schematic View of Optical System of White Light Interferometry [69]

In this study, white light interferometer is used to measure the surface roughness of the finish-turned PC specimens as shown in Figure 3.15 and technical specifications are given in Appendix E.



Figure 3.15 Zygo NewView 5000 White Light Interferometry [70]

The surface roughness of machined PC specimens are measured in terms of three different parameters. Peak to Valley, root-mean-squared roughness and average roughness values of the surfaces are obtained from the interferometry measurements. Since any residual dirt, dust, grime or other absorbent materials left on the surface can highly affect the measurements, all measurements are done after the cleaning the surfaces of turned PC specimens.

3.8 Machining Parameters and Experimental Procedure

In this study, totally 43 runs are performed. In the first part of the experiment, 27 PC specimens are cut in 27 different machining conditions depending on three-level full factorial design which was clarified in Chapter 3.2. Feed rate, spindle speed and depth of cut are selected between 1-9 $\mu\text{m}/\text{rev}$, 1000-2000 rpm and 5-40 μm respectively as cutting conditions. After completing every five runs, the first run is repeated by using cutting conditions which is 5 $\mu\text{m}/\text{rev}$ feed rate, 2000 rpm spindle speed and 40 μm depth of cut, in

order to control the tool wear. In the second part, one PC specimen is cut three times by using same cutting conditions which is 5 $\mu\text{m}/\text{rev}$ feed rate, 2000 rpm spindle speed and 5 μm depth of cut, in order to show the repeatability of the experiment. In the final part, using the same experimental setups, a validation run is performed. One PC specimen is cut in 8 different cutting conditions which feed rate, spindle speed and depth of cut are selected between 2-12 $\mu\text{m}/\text{rev}$, 1000-2250 rpm and 3-50 μm , respectively. The range of the parameters in validation run is selected bigger than that of experimental runs. The main objective was to show the reaction of the model for different cutting conditions and to learn the tendency of response beyond the limits.

After the adjustment of tool and workpiece setup, the finish cutting of flat polycarbonate specimens with mono-crystalline diamond tool were performed. After all cutting operations, the surface roughness of each PC flat disc specimen is measured by using white light interferometer from 4 different points, all in 90° with each other across the circumference as shown in Figure 3.16.

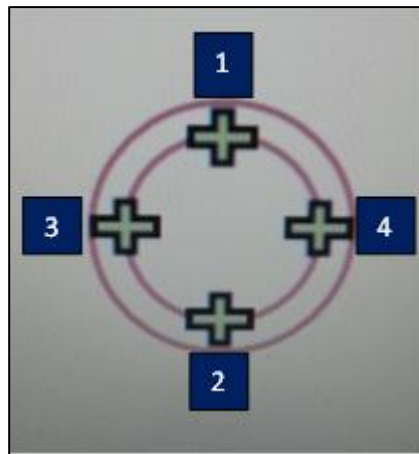


Figure 3.16 Measurement points for PC specimen

After completing all runs, three-level full factorial design method was performed to obtain a mathematical relation between surface roughness and surface parameters. This method is conducted by SAS Institute JMP statistical software. Then, ANN modeling was performed to predict the surface roughness for experimental runs and validation runs.

During each cutting, the vibration data is collected in x,y, and z direction by using the vibration data collection system. A SPSS analysis is used to determine the Pearson's correlations between the vibration data in x, y, and z directions and surface roughness.

An independent samples t-test was also implemented to analyze the results of ANN predictions by using IBM SPSS Statistics 20 software.

As a result, the surface roughness values of machined polycarbonate specimens were measured and mathematical models are obtained by using the results of different experimental design methods and these results are analyzed. The repeatability of the experiment is analyzed and a validation run is performed to check the surface roughness results predicted by ANN model and full factorial design method.

3.9 Three-Level Full Factorial Design

Three-level experimental design method is performed to obtain a mathematical model and find the relationship between cutting parameters and surface roughness. During machining, the highest, the lowest, and the middle values of machining parameters are used. Feed rate, depth of cut and spindle speed are selected to define a relationship between surface roughness and machining parameters.

During machining Kerosene with misted air is used as cutting fluid. Mono-crystalline diamond tool whose tooling number is S95843 of Contour was chosen as 0° rake angle and 10° clearance angle according to previous studies and manufacturer’s suggestions. The properties of cutting fluid and tool were given in Table 3-3.

Table 3-3 Machining Parameters for Experiment 1

Cutting Fluid	Dovent IP 175/195
Mono-crystalline Diamond Tool	S95843 – C020LG
Nose Radius (mm)	0.5
Rake Angle (°)	0
Clearance Angle (°)	10

The first experimental study is performed by 3 Level Full Factorial Design with three parameters and flat polycarbonate disk was machined at highest, lowest and center point of each parameters. The order of runs are given in Table 3-4.

Table 3-4 Order of Runs for the Experiment 1

Run	Feed Rate ($\mu\text{m}/\text{rev}$)	Depth of Cut (μm)	Spindle Speed (RPM)
1	5	40	2000
2	9	22.5	1000
3	5	22.5	2000
4	9	22.5	2000
5	9	5	1500
6	5	5	2000
7	1	40	1000
8	1	5	2000
9	1	40	2000
10	5	5	1500
11	1	22.5	2000
12	1	40	1500
13	5	22.5	1000
14	1	5	1500

Run	Feed Rate ($\mu\text{m}/\text{rev}$)	Depth of Cut (μm)	Spindle Speed (RPM)
15	5	40	1000
16	5	5	1000
17	9	5	1000
18	1	22.5	1000
19	1	5	1000
20	5	22.5	1500
21	5	40	1500
22	9	40	2000
23	9	40	1000
24	1	22.5	1500
25	9	40	1500
26	9	5	2000
27	9	22.5	1500

Totally, 27 runs are performed as shown in Table 3-5. Four different points with 90° angle are used as measurement points and the average of these four values are taken as average roughness. The best and the worst surface roughness measurements from Zygo Interferometry are given in Appendix F. The measurement results for all runs are tabulated in Appendix G and Appendix H.

Table 3-5 Results of the Surface Roughness Measurements for Experiment 1

Run	Feed Rate ($\mu\text{m}/\text{rev}$)	Depth of Cut (mm)	Spindle Speed (RPM)	R_a (nm)	rms (nm)	PV (nm)
1	5	40	2000	17.9	27.5	749.3
2	9	22.5	1000	15.0	17.6	399.9
3	5	22.5	2000	16.5	29.3	566.9
4	9	22.5	2000	33.7	64.2	1101.9
5	9	5	1500	19.7	25.8	679.6
6	5	5	2000	9.4	12.1	544.2
7	1	40	1000	10.1	12.9	265.7
8	1	5	2000	2.7	3.4	32.7
9	1	40	2000	9.5	12.0	150.9
10	5	5	1500	12.0	16.0	634.0
11	1	22.5	2000	6.4	8.0	67.7
12	1	40	1500	9.2	11.5	167.0
13	5	22.5	1000	12.2	15.2	126.4
14	1	5	1500	3.7	4.7	55.6
15	5	40	1000	12.8	16.0	359.3
16	5	5	1000	10.2	13.0	277.7
17	9	5	1000	11.5	18.6	792.7
18	1	22.5	1000	8.3	10.5	163.3
19	1	5	1000	4.7	7.8	143.6
20	5	22.5	1500	8.5	10.9	315.1
21	5	40	1500	13.6	17.5	489.6
22	9	40	2000	46.8	97.4	1565.4
23	9	40	1000	25.9	57.6	1357.9
24	1	22.5	1500	4.3	5.5	186.5
25	9	40	1500	21.6	48.8	1412.0
26	9	5	2000	22.1	50.4	1225.4
27	9	22.5	1500	26.4	62.8	1471.7

The mathematical relationship between R_a and machining parameters for 3^3 full factorial design used in this study is shown below [57].

$$Y(ijk) = \mu + A(i) + B(j) + AB(ij) + C(k) + AC(ik) + BC(jk) + ABC(ijk) \quad (3.1)$$

The open-form of Equation (3.1) which has 17 coefficients from a_0 to a_{123} is formulated as in Equation (3.2). All these coefficients are calculated by using JMP® Pro 10. The calculated coefficients for R_a , R_q and PV are given in Table 3.6.

$$\begin{aligned} R = & a_0 + a_1 * f + a_2 * doc + a_3 * S + a_{12} * f * doc + a_{13} * f * S \\ & + a_{23} * doc * S + a_{11} * f * f + a_{22} * doc * doc + a_{33} * S * S \\ & + a_{112} * f * f * doc + a_{113} * f * f * S + a_{221} * S * S * f \\ & + a_{223} * doc * doc * S + a_{331} * S * S * f + a_{332} * S * S * doc \\ & + a_{123} * f * doc * S \end{aligned} \quad (3.2)$$

Where;

R: Roughness (R_a , R_q and PV)

f: Feed rate

doc: Depth of cut

S: Spindle speed

Table 3-6 The coefficients for 3^3 full factorial design

Coefficient	PV	rms	R_a
a_0	566.731	25.067	14.608
a_1	397.983	16.640	7.424
a_2	-0.628	-3.261	-1.608
a_3	96.071	6.138	2.463
a_{12}	-5.017	-2.314	-0.770
a_{13}	92.415	6.989	3.040
a_{23}	-25.476	-1.759	-0.738
a_{11}	81.577	5.356	1.451
a_{22}	-111.281	-5.929	-2.821
a_{33}	-24.392	1.739	0.982
a_{112}	-43.495	-0.934	-0.594
a_{113}	-37.625	1.953	0.920
a_{221}	-79.603	-4.339	-1.050
a_{223}	21.488	-0.528	-0.704
a_{331}	-22.093	0.638	0.383
a_{332}	57.680	0.829	-0.764
a_{123}	-17.273	-0.873	-0.541

Since the parameter levels were selected as -1,0 and 1, the equation above can not be used for actual cutting parameter values. Therefore, a transformation is made for using actual cutting parameters in engineering units as shown in Equation (3.3).

$$\begin{aligned}
R = & a_0 + a_1 * [(f - 5) / 4] + a_2 * [(doc - 22.5) / 17.5] \\
& + a_3 * [(S - 1500) / 500] + a_{12} * [(f - 5) / 4] * [(doc - 22.5) / 17.5] \\
& + a_{13} * [(f - 5) / 4] * [(S - 1500) / 500] \\
& + a_{23} * [(doc - 22.5) / 17.5] * [(S - 1500) / 500] \\
& + a_{11} * [(f - 5) / 4] * [(f - 5) / 4] \\
& + a_{22} * [(doc - 22.5) / 17.5] * [(doc - 22.5) / 17.5] \\
& + a_{33} * [(S - 1500) / 500] * [(S - 1500) / 500] \\
& + a_{112} * [(f - 5) / 4] * [(f - 5) / 4] * [(doc - 22.5) / 17.5] \\
& + a_{113} * [(f - 5) / 4] * [(f - 5) / 4] * [(S - 1500) / 500] \\
& + a_{221} * [(S - 1500) / 500] * [(S - 1500) / 500] * [(f - 5) / 4] \\
& + a_{223} * [(doc - 22.5) / 17.5] * [(doc - 22.5) / 17.5] * [(S - 1500) / 500] \\
& + a_{331} * [(S - 1500) / 500] * [(S - 1500) / 500] * [(f - 5) / 4] \\
& + a_{332} * [(S - 1500) / 500] * [(S - 1500) / 500] * [(doc - 22.5) / 17.5] \\
& + a_{123} * [(f - 5) / 4] * [(doc - 22.5) / 17.5] * [(S - 1500) / 500]
\end{aligned} \tag{3.3}$$

By using Equation (3.3), the predicted R_a values are calculated and the comparison with measured R_a is tabulated in Table 3-7. The comparison between measured and predicted PV and R_q values are given in Table 3-8. Then, prediction accuracy for three-level full factorial design are determined. Equation (3.4) is used to calculate the accuracy of the model.

$$\delta = \frac{1}{n} \sum_{i=1}^n \left(\frac{R_{a,i} - R_{a,i}^p}{R_{a,i}} \times 100\% \right) \tag{3.4}$$

where

δ = the estimation error

n = the total number of measurements

i = the estimated measurement for a specific run

$R_{a,i}$ = the measured surface roughness for a specific run

$R_{a,i}^p$ = the predicted surface roughness for a specific run

Table 3-7 Comparison of measured and predicted R_a values

Run	Measured R_a (nm)	Predicted R_a (nm)	Residual (nm)	Error (%)
1	17.9	19.2	-1.3	7.50
2	15.0	17.3	-2.3	15.50
3	16.5	14.9	1.5	9.24
4	33.7	35.0	-1.4	4.07
5	19.7	18.1	1.6	8.03
6	9.4	9.5	-0.2	1.95
7	10.1	10.8	-0.7	6.58
8	2.7	0.4	2.3	86.28
9	9.5	11.7	-2.2	22.74
10	12.0	11.9	0.2	1.28
11	6.4	6.6	-0.2	2.36
12	9.2	6.3	2.8	30.90
13	12.2	11.1	1.1	8.78
14	3.7	5.4	-1.7	47.51
15	12.8	13.9	-1.1	8.56
16	10.2	10.1	0.0	0.28
17	11.5	10.9	0.6	4.86
18	8.3	7.1	1.3	15.04
19	4.7	5.3	-0.6	12.42
20	8.5	11.1	-2.6	30.41
21	13.6	11.2	2.4	17.92
22	46.8	43.3	3.5	7.49
23	25.9	24.1	1.8	6.81
24	4.3	5.4	-1.1	25.55
25	21.6	26.8	-5.3	24.45
26	22.1	24.2	-2.1	9.69
27	26.4	22.8	3.7	13.96

Table 3-8 Comparison of measured and predicted R_q and PV values

Run	Measured R_q (nm)	Predicted R_q (nm)	Residual R_q (nm)	Error rate rms (%)	Measured PV (nm)	Predicted PV (nm)	Residual PV (nm)	Error rate PV (%)
1	27.5	29.3	-1.7	6.29	749.3	698.8	50.5	6.74
2	17.6	26.0	-8.4	47.84	399.9	605.5	-205.5	51.39
3	29.3	24.1	5.1	82.42	566.9	494.5	72.4	87.22
4	64.2	69.8	-5.6	108.79	1101.9	1166.5	-64.6	105.86
5	25.8	29.3	-3.4	113.36	679.6	909.8	-230.2	133.87
6	12.1	15.5	-3.4	128.18	544.2	667.1	-122.9	122.59
7	12.9	15.6	-2.8	121.66	265.7	320.1	-54.5	120.50
8	3.4	1.0	2.4	29.83	32.7	37.2	-4.5	113.59
9	12.0	14.9	-2.9	124.05	150.9	138.6	12.3	91.87
10	16.0	12.1	3.9	75.74	634.0	448.1	185.9	70.68
11	8.0	7.5	0.5	93.85	67.7	75.5	-7.8	111.55
12	11.5	5.8	5.7	50.49	167.0	124.8	42.2	74.74
13	15.2	11.5	3.7	75.74	126.4	15.2	111.2	11.99
14	4.7	5.2	-0.4	109.23	55.6	11.3	44.3	20.37
15	16.0	19.2	-3.2	120.08	359.3	407.5	-48.3	113.44
16	13.0	13.4	-0.5	103.66	277.7	340.6	-63.0	122.67
17	18.6	16.2	2.4	86.93	792.7	689.9	102.8	87.03
18	10.5	5.7	4.7	54.61	163.3	69.0	94.3	42.23
19	7.8	9.8	-2.0	125.16	143.6	183.5	-39.9	127.75
20	10.9	19.8	-8.8	180.62	315.1	498.8	-183.7	158.29
21	17.5	12.6	4.9	71.83	489.6	491.8	-2.2	100.45
22	97.4	92.8	4.6	95.25	1565.4	1628.2	-62.8	104.01
23	57.6	51.6	6.0	89.60	1357.9	1255.2	102.7	92.44
24	5.5	10.7	-5.2	195.82	186.5	273.0	-86.5	146.38
25	48.8	59.4	-10.6	121.76	1412.0	1452.0	-40.0	102.83
26	50.4	49.4	1.0	97.99	1225.4	1098.1	127.4	89.61
27	62.8	48.7	14.1	77.59	1471.7	1201.5	270.1	81.64

By using the formula in Equation (3.4) and the results in Table 3-7, the error rate of this model is calculated to be 15.93%.

Finally, an ANOVA study is conducted with JMP® Pro 10 to analyze the effect of the parameters. A low p-value as 0.0015 and the coefficient of determination (r^2) as 0.96 show a statistically significant effect on surface roughness among the factors. Summary of fit, analysis of variance and F-tests for model and for parameters are tabulated in Table 3-9 through Table 3-11.

In Table 3-9, correlation coefficient of the model is about 0.96 which shows that the parameters in the model significantly affect the result. Low P-value in Table 3-10 indicates that our null hypothesis that none of the parameters affect the result, is not true. This low value says that at least one of the parameters is significantly related to the result.

Table 3-9 Summary of Fit

Summary of Fit	
RSquare	0.9551528
RSquare Adj	0.8542466
Root Mean Square Error	3.7969396
Mean of Response	14.608185
Observations (or Sum Wgts)	27

Table 3-10 ANOVA for prediction model

Source	DF	Sum of Squares	Mean Square	F Ratio	Prob>F
Model	18	2456.3762	136.465	9.4657	0.0015
Error	8	115.334	14.417		
C. Total	26	2571.7102			

Table 3-11 F-Test for factors

Source	Nparm	DF	Sum of Squares	F Ratio	Prob>F
f(um/rev)	2	2	1544.8943	53.5798	<.0001
doc(um)	2	2	284.6509	9.8722	0.0069
S(RPM)	2	2	189.7873	6.5822	0.0204
f(um/rev)*doc(um)	4	4	76.628	1.3288	0.3384
f(um/rev)*S(RPM)	4	4	276.6786	4.7979	0.0286
doc(um)*S(RPM)	4	4	83.7372	1.4521	0.3022

In Table 3-11, the effects of factors and their interactions on surface roughness are highlighted. Feed rate is the most dominant effect on surface roughness due to low P-value. Depth of cut, spindle speed and the interaction between feed rate and spindle speed have also effect on surface roughness even if their effect is not as high as that of feed rate.

3.10 Artificial Neural Network Modeling

In this section, a method used to make use of the vibration data in prediction of the surface roughness is presented. Since the correlation is a measure of how well the parameters are related, Pearson’s correlations, the most common measure of correlation in statistics, between surface roughness and cutting parameters including vibration data are determined by using IBM SPSS Statistics 20 software and standard deviations and Pearson Correlation coefficients are tabulated in Table 3-12 and Table 3-13.

Table 3-12 Descriptive Statistics for Vibration and Surface Roughness

	Mean	Std. Deviation	N
Ra	14.60819	9.945448	27
Vx	27.39374	2.524430	27
Vy	52.15826	7.301313	27
Vz	37.64059	4.320149	27

Table 3-13 Pearson's Correlations for Vibration Data

		Ra	Vx	Vy	Vz
Ra	Pearson Correlation	1	.578**	.553**	.566**
	Sig. (2-tailed)		.002	.003	.002
	Sum of Squares and Cross-products	2,571.710	377.106	1,044.452	632.471
	Covariance	98.912	14.504	40.171	24.326
	N	27	27	27	27
Vx	Pearson Correlation	.578**	1	.800**	.683**
	Sig. (2-tailed)	.002		.000	.000
	Sum of Squares and Cross-products	377.106	165.691	383.485	193.717
	Covariance	14.504	6.373	14.749	7.451
	N	27	27	27	27
Vy	Pearson Correlation	.553**	.800**	1	.611**
	Sig. (2-tailed)	.003	.000		.001
	Sum of Squares and Cross-products	1,044.452	383.485	1,386.039	501.123
	Covariance	40.171	14.749	53.309	19.274
	N	27	27	27	27
Vz	Pearson Correlation	.566**	.683**	.611**	1
	Sig. (2-tailed)	.002	.000	.001	
	Sum of Squares and Cross-products	632.471	193.717	501.123	485.256
	Covariance	24.326	7.451	19.274	18.664
	N	27	27	27	27

** . Correlation is significant at the 0.01 level (2-tailed).

Analyzing the Pearson Correlation values for V_x , V_y , and V_z , SPSS analysis showed that vibration in three directions is also an important factor on surface roughness. Pearson's correlations for feed rate, depth of cut and spindle speed are also represented to compare the effects of all parameters. Table 3-14 represents the results of SPSS analysis for cutting parameters. According to these results, feed rate is the most significant factor since the Pearson's Correlation coefficient is 0.761 which is much bigger than that of depth of cut and spindle speed.

Table 3-14 Pearson's Correlations for Cutting Parameters

		Ra	feedrate	depthofcut	spindlespeed
Ra	Pearson Correlation	1	.761**	.333	.252
	Sig. (2-tailed)		.000	.090	.204
	Sum of Squares and Cross-products	2,571.710	654.636	1,252.633	27,144.500
	Covariance	98.912	25.178	48.178	1,044.019
	N	27	27	27	27
feedrate	Pearson Correlation	.761**	1	.000	.000
	Sig. (2-tailed)	.000		1.000	1.000
	Sum of Squares and Cross-products	654.636	288.000	.000	.000
	Covariance	25.178	11.077	.000	.000
	N	27	27	27	27
depthofcut	Pearson Correlation	.333	.000	1	.000
	Sig. (2-tailed)	.090	1.000		1.000
	Sum of Squares and Cross-products	1,252.633	.000	5,512.500	.000
	Covariance	48.178	.000	212.019	.000
	N	27	27	27	27
spindlespeed	Pearson Correlation	.252	.000	.000	1
	Sig. (2-tailed)	.204	1.000	1.000	
	Sum of Squares and Cross-products	27,144.500	.000	.000	4,500,000.000
	Covariance	1,044.019	.000	.000	173,076.923
	N	27	27	27	27

** . Correlation is significant at the 0.01 level (2-tailed).

ANN has become a part of this thesis in that point since the analysis will be very difficult to carry out including vibration data. Using ANN, such a variety of parameters can be experimented fast and accurately. As explained in detail in Chapter 3, the number of hidden neurons in the layer was the only parameter which will be changed in that ANN approach. From 1 to 10 hidden neurons are experimented for this study and best network which gives the best prediction have been found. Matlab 7.9.0 with Neural Fitting Tool (nftool) interface has been used during the ANN modeling. All results have been presented by using sim function which simulates the neural networks.

In ANN modeling, three different groups are defined for the system. Firstly, 27 input data set with 6 variables were entered to the system. Secondly, the results of these 27 runs are added to the system as target. Finally, a validation set with 6 parameters are selected to predict. The data set defined for the system is shown in Table 3-15.

Table 3-15 Input and Target Data Set for ANN modeling

Run	Feed Rate	Depth of Cut	Spindle Speed	X	Y	Z	R _a
	($\mu\text{m}/\text{rev}$)	(μm)	(RPM)	(mgRMS)	(mgRMS)	(mgRMS)	(nm)
1	5	40	2000	28.07	45.97	41.69	17.9
2	9	22.5	1000	27.9	52.76	37.75	15.0
3	5	22.5	2000	27.86	44.58	38.87	16.5
4	9	22.5	2000	29.9	61.7	46.74	33.7
5	9	5	1500	26.97	43.16	37.54	19.7
6	5	5	2000	25.35	49.91	35.04	9.4
7	1	40	1000	28.74	44.8	39.13	10.1
8	1	5	2000	25.17	45.21	32.67	2.7
9	1	40	2000	26.54	56.23	35.81	9.5
10	5	5	1500	27.09	52.08	36.9	12.0
11	1	22.5	2000	26.45	52.67	36.93	6.4
12	1	40	1500	28.75	52.6	35.59	9.2
13	5	22.5	1000	26.72	52.41	37.35	12.2
14	1	5	1500	25.53	46.66	33.04	3.7
15	5	40	1000	32.77	66.69	38.66	12.8
16	5	5	1000	28.91	58.81	46.34	10.2
17	9	5	1000	26.06	54.75	35.74	11.5
18	1	22.5	1000	25.88	48.86	33.23	8.3
19	1	5	1000	28.14	54.58	37.88	4.7
20	5	22.5	1500	25.15	46.91	33.72	8.5
21	5	40	1500	26.01	50.85	40.1	13.6
22	9	40	2000	36.22	74.97	45.09	46.8
23	9	40	1000	25.64	48.615	33.207	25.9
24	1	22.5	1500	25.25	44.57	33.09	4.3
25	9	40	1500	25.61	48.27	33.2	21.6
26	9	5	2000	24.65	50.64	34.67	22.1
27	9	22.5	1500	28.301	59.018	46.319	26.4

The ANN models are designed depending on the values above. The back-propagation algorithm is used to adjust the weights of the hidden layer neurons. Transfer function of the model is selected as the sigmoid function as mentioned before. A network with 6 hidden neurons is selected for giving the minimum mean percentage error for all runs. The error rate for the model which has 6 hidden neurons is 5.14%, which is an acceptable ratio for a complex process. Figure 3.17 indicates the difference between measured and predicted data. The comparison of results which are obtained from different number of hidden neurons are tabulated in Table 3-16 according to their prediction accuracy. In this table, the effect of number of hidden neurons are analyzed in terms of prediction accuracy.

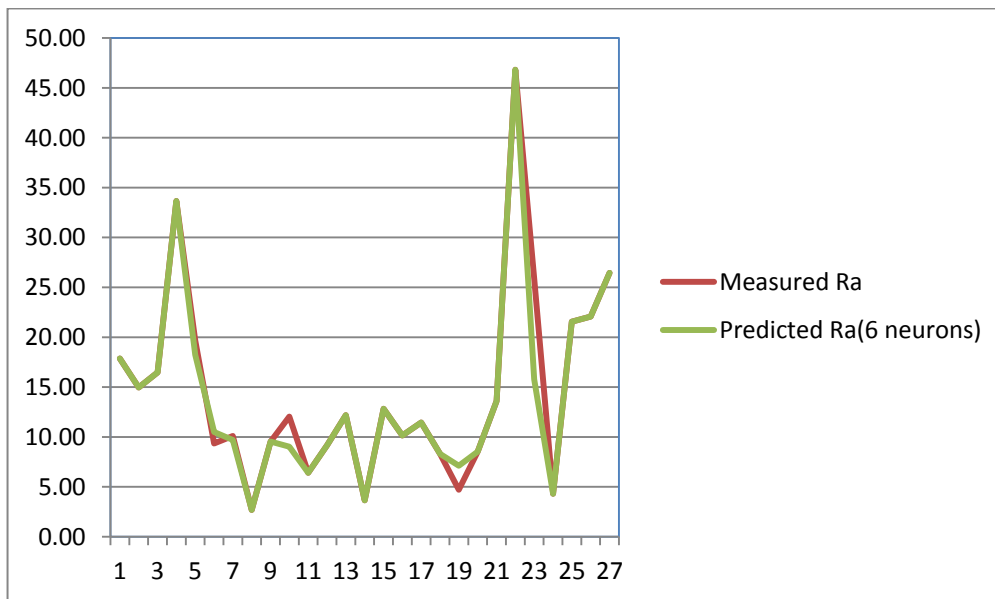


Figure 3.17 Comparison of the measured surface roughness and predicted surface roughness of ANN model

Table 3-16 Surface Roughness Predictions using different number of neurons

Run	Measured R _a (nm)	Number of hidden neurons for Prediction of Average Surface Roughness									
		1	2	3	4	5	6	7	8	9	10
1	17.9	20.7	18.1	18.0	18.4	20.1	17.9	17.9	18.6	17.9	18.0
2	15.0	17.9	19.2	15.4	19.4	19.3	15.0	15.0	15.0	15.0	13.0
3	16.5	15.3	15.0	16.1	16.4	15.7	16.5	16.1	16.6	16.5	17.6
4	33.7	33.7	33.9	33.7	33.9	33.3	33.7	33.7	33.7	34.0	32.5
5	19.7	17.4	20.0	19.0	21.9	18.8	18.2	21.9	19.4	19.7	20.1
6	9.4	10.1	9.9	9.5	10.6	9.9	10.5	10.5	11.1	8.3	11.1
7	10.1	7.1	9.7	10.1	9.9	10.1	9.7	10.1	10.4	10.1	9.1
8	2.7	6.4	3.9	5.9	4.3	3.6	2.7	0.5	2.4	2.7	4.3
9	9.5	9.1	9.2	9.3	9.8	8.3	9.5	9.5	7.3	9.5	9.5
10	12.0	8.8	10.7	11.6	9.1	10.4	9.0	12.0	11.5	12.0	11.8
11	6.4	7.6	7.1	6.8	5.1	6.0	6.4	5.4	6.5	6.4	7.1
12	9.2	8.1	9.3	8.9	10.4	8.8	9.2	9.2	9.3	9.2	8.7
13	12.2	8.7	11.0	13.4	12.9	10.9	12.2	12.2	12.4	12.2	10.2
14	3.7	5.9	3.9	5.9	3.9	3.5	3.7	3.7	3.6	3.7	3.6
15	12.8	14.1	13.3	12.9	13.2	13.1	12.8	12.8	12.9	12.8	13.3
16	10.2	8.2	10.9	9.8	10.0	11.5	10.2	10.2	9.4	10.2	10.5
17	11.5	12.3	15.2	10.2	12.7	14.1	11.5	11.5	11.3	10.7	12.2
18	8.3	5.9	7.2	6.2	8.0	7.0	8.3	11.0	8.4	8.3	6.8
19	4.7	5.7	6.8	4.8	3.4	4.9	7.1	4.7	4.5	4.7	5.6
20	8.5	10.0	11.6	10.1	9.5	11.8	8.5	8.5	10.8	8.5	7.4
21	13.6	13.9	13.9	13.2	17.3	16.6	13.6	13.6	13.9	13.0	11.9
22	46.8	44.8	44.3	46.7	44.0	51.8	46.8	46.8	46.8	46.8	45.9
23	25.9	20.2	20.6	23.6	24.7	29.1	15.8	25.9	26.1	25.9	20.9
24	4.3	6.4	6.1	6.0	4.1	6.0	4.3	4.3	2.1	9.0	3.5
25	21.6	26.1	25.6	24.0	21.4	29.6	21.6	21.6	21.7	25.2	25.0
26	22.1	19.7	21.6	21.6	21.6	20.2	22.1	22.1	21.5	22.1	20.8
27	26.4	25.5	26.1	27.5	26.6	27.8	26.4	26.4	31.9	26.4	26.0
Mean Error Percentage(MEP)		22.17	13.51	12.84	10.95	13.96	5.14	5.79	7.08	5.56	10.75

3.11 Comparison of Experimental Methods

In this section, the comparison between 3-level full factorial design and ANN modeling will be carried out. Both methods have been performed for the diamond turning of PC disks and prediction models have been obtained. In both cases, 27 runs were performed and feed rate, depth of cut and spindle speed has been used as cutting parameters. However, ANN modeling utilized vibration data, as well after SPSS analysis. Pearson's correlations. The main purpose of 3-level full factorial design is to find the most significant factors on the response and determine the weights of all factors. Then, a prediction model can be obtained according to the weights of these parameters. However, ANN modeling is concentrated to design the optimum network for the prediction of response. It does not compare the effects of input parameters but the user can compare the effects by giving different input data sets to the model. For example, the prediction error of the model for the surface roughness of 27 cases is 14.99% if only feed rate, depth of cut and spindle speed were used as inputs without vibration inputs. The error rate has been calculated as 15.93% by 3-level full factorial design. Therefore, full factorial design has also made reasonable predictions by using only three input parameters.

In the second part of the experiment, 8 validation runs have been performed. In these runs, parameters have been selected randomly and some of the values of the parameters were beyond the range which was studied in 27 run experiment. The purpose for doing that was observing the tendency of model for different inputs. Table 3-17 shows the inputs for the second part of the experiment.

Table 3-17 Input data set for 8 runs

Run	Feed Rate ($\mu\text{m}/\text{rev}$)	Depth of Cut (μm)	Spindle Speed (rpm)
1	2	3	1250
2	7	22	1000
3	12	10	1750
4	2	6	2250
5	7	30	1750
6	12	40	1250
7	2	50	1000
8	7	20	2250

The results of surface roughness and vibration measurements in three directions have been tabulated in Table 3-18.

Table 3-18 Surface roughness and vibration measurements for validation runs

Run	Feed Rate ($\mu\text{m}/\text{rev}$)	Depth of Cut (μm)	Spindle Speed (rpm)	Ra (nm)	PV (nm)	rms (nm)	X (mgRMS)	Y (mgRMS)	Z (mgRMS)
1	2	3	1250	6.9	246.3	8.7	28.61	59.82	47.17
2	7	22	1000	18.1	780.9	30.2	28.63	59.83	46.42
3	12	10	1750	47.7	1640.8	96.6	28.16	58.97	47.48
4	2	6	2250	6.3	79.1	8.0	28.76	60.88	49.09
5	7	30	1750	23.0	1033.2	43.5	37.26	78.91	54.13
6	12	40	1250	52.1	1855.6	106.7	28.59	59.90	46.48
7	2	50	1000	5.8	229.7	7.8	28.92	60.00	46.70
8	7	20	2250	14.4	955.8	23.5	28.91	59.77	46.93

After completing measurements, the prediction capability of experimental designs has been investigated. The prediction formula for 3-level full factorial design had been obtained in Chapter 3. By using that formula, the predicted data was calculated for 8 validations. Also, the network with 6 hidden neurons has been recalculated for the new data set. The predicted average roughness values have been shown in Table 3-19.

Table 3-19 Predicted Average Surface Roughness Values

Run	Feed Rate ($\mu\text{m}/\text{rev}$)	Depth of Cut (μm)	Spindle Speed (rpm)	Measured Ra (nm)	Predicted Ra by ANN Modeling (nm)	Predicted Ra by 3-level full factorial design (nm)
1	2	3	1250	6.9	5.2	9.1
2	7	22	1000	18.1	14.2	15.7
3	12	10	1750	47.7	33.3	39.4
4	2	6	2250	6.3	6.8	13.1
5	7	30	1750	23.0	17.6	19.2
6	12	40	1250	52.1	35.0	18.7
7	2	50	1000	5.8	5.1	3.8
8	7	20	2250	14.4	24.2	28.3

Finally, the error rate of ANN modeling and 3-level full factorial design has been found as 27.5% and 48.17%, respectively. Although the uncontrollable disturbances like vibration make the prediction process much more difficult, the predictions above can be interpreted as useful information. For example, ANN modeling guessed the average surface roughness with 27.5% error. However, the mean of predicted surface roughness in validation run is about 17 nm, so 27.5% error makes the guesses about ± 5 nm away from the measured values. That is why, ANN modeling can be used for the prediction of surface roughness in diamond turning if the desired output will not be sensitive as ± 5 nm. When there is need for more sensitive surface roughness predictions, much more input data must be entered to the system so that ANN modeling can train the system effectively.

3.12 Repeatability of the Experiment

In addition to testing and validation of experiments, two more experiments are carried out. In the first experiment, which is planned to check the repeatability, during the runs given in Table 3-4, the first run whose cutting conditions as $5\mu\text{m}/\text{rev}$ feed rate, $40\mu\text{m}$ depth of cut and 2000 rpm spindle speed, is repeated after every 5 runs. The results of cuts are shown in Table 3-20.

Table 3-20 Repetition of 1st run after every 5 runs

Run	Feed Rate	Depth of Cut	Spindle Speed	R _a	PV	rms	X	Y	Z
	($\mu\text{m}/\text{rev}$)	(μm)	(RPM)	(nm)	(nm)	(nm)	(mgRMS)	(mgRMS)	(mgRMS)
R-1	5	40	2000	17.9	749.3	27.5	28.07	45.97	41.69
R-2	5	40	2000	21.6	873.8	35.9	29.9	61.7	46.74
R-3	5	40	2000	16.1	585.3	21.1	29.56	60.19	41.94
R-4	5	40	2000	12.9	488.9	16.1	28.6	53.5	38.82
R-5	5	40	2000	16.8	669.1	21.3	29.09	47.52	40.26
R-6	5	40	2000	8.4	185.3	10.8	25.39	44.99	33.38

Analyzing these results, surface roughness values are nearly the same for three different runs whose numbers are R-1,R-3 and R-5. However, the other runs result in different surface roughness values. When the data is carefully analyzed, it is clear that vibration data for the runs are differ in some way. For example, 30th run has a relatively low surface roughness value and looking at vibration information, it is clear that small vibration amplitude has positive effect on surface roughness. On the other hand, 6th run has relatively high surface roughness but not surprisingly it has the highest vibration amplitude in all directions. Therefore, vibration has showed a significant effect on surface roughness as expected, although the cutting parameters are the same.

In the second experiment, one specimen is cut three times by using the same cutting conditions. For this random cut; feed rate, depth of cut and spindle speed are selected as 2 $\mu\text{m}/\text{rev}$, 5 μm , and 2000 rpm, respectively. The results of this experiment are shown in Table 3-21. The surface roughness values for these three successive cuts appeared to be the same and the vibration data is also close for these runs.

Table 3-21 Measurements results of one PC specimen after successive cuttings

Run	Feed Rate	Depth of Cut	Spindle Speed	R _a	PV	rms	X	Y	Z
	($\mu\text{m}/\text{rev}$)	(μm)	(RPM)	(nm)	(nm)	(nm)	(mgRMS)	(mgRMS)	(mgRMS)
M-1	2	5.0	2000	6.41	93.28	8.22	29.798	60.416	47.608
M-2	2	5.0	2000	6.59	205.68	8.44	27.642	60.727	49.204
M-3	2	5.0	2000	6.92	607.44	9.43	28.459	60.263	48.574

At the end of the experiment, surface roughness measurement for the 3rd run in Table 3-21 is repeated to show the sensitivity of measurement process. The results are tabulated in Table 3-22.

Table 3-22 Repetition of Surface Roughness Measurement for 3rd run

Run	Position #	Ra-1	PV-1	rms-1	Ra-2	PV-2	rms-2
		(nm)	(nm)	(nm)	(nm)	(nm)	(nm)
3	1	6.552	399.305	8.737	6.945	112.799	8.975
	2	6.801	542.953	9.277	6.357	84.164	8.101
	3	6.924	1,083.454	9.755	7.341	406.740	9.885
	4	7.420	404.051	9.937	6.847	89.306	8.734
	Average	6.924	607.441	9.427	6.873	173.252	8.924

CHAPTER 4

INTERPRETATION OF EXPERIMENTAL RESULTS

4.1 Introduction

In this chapter, the influence of feed rate, depth of cut and spindle speed on surface roughness will be analyzed. Then, the effect of vibration on surface roughness will be analyzed for different cutting conditions. Moreover, the results of three-level full factorial design will be highlighted, and leverage plots for cutting parameters which has been gathered from JMP analysis will be presented.

4.2 Effect of Feed Rate

Pearson's correlation and ANOVA analysis in Chapter 3 indicated the influence of feed in diamond turning of polycarbonate. In literature, it is also indicated that feed rate is the most significant cutting parameter in different cutting conditions. Cutting material changes, process variables change, environmental conditions change but the effect of feed rate is always prominent.

Leverage plots show that small feed rate gives better surface roughness and increasing feed rate diminishes the quality of the surface. Figure 4.1 shows the distribution of surface roughness with varying feed rate. As explained in Chapters 3, feed rate has been changed from 1 $\mu\text{m}/\text{rev}$ to 9 $\mu\text{m}/\text{rev}$ and the mean surface roughness at each feed rate is tabulated in Table 4-1.

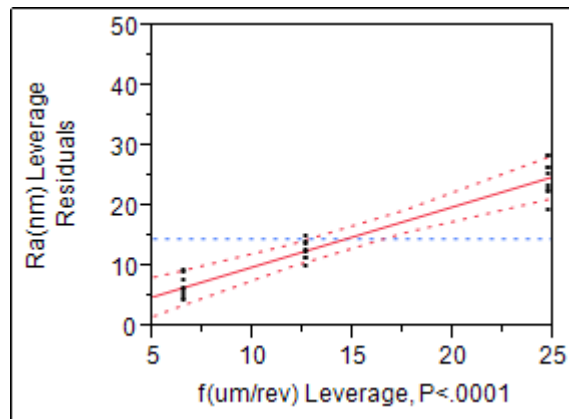


Figure 4.1 Leverage plot for feed rate

Table 4-1 Least Squares Means Table for feed rate

Level	Least Sq Mean	Std Error	Mean
1.00	6.54	1.266	6.542
5.00	12.56	1.266	12.556
9.00	24.73	1.266	24.727

According to 27- runs testing experiment, the variation of surface roughness with feed rate is given in Figure 4.2 while depth of cut and spindle speed are kept constant for every 3 runs. This figure shows a strong relation between surface roughness and feed rate. For 8- runs validation experiment, similar results have been obtained as shown in Figure 4.3. Pearson's correlation results which had been shown in Table 3-14, also showed that feed rate is the most important parameter on surface roughness. Therefore, controlling the feed rate is the primary task to achieve better surface quality.

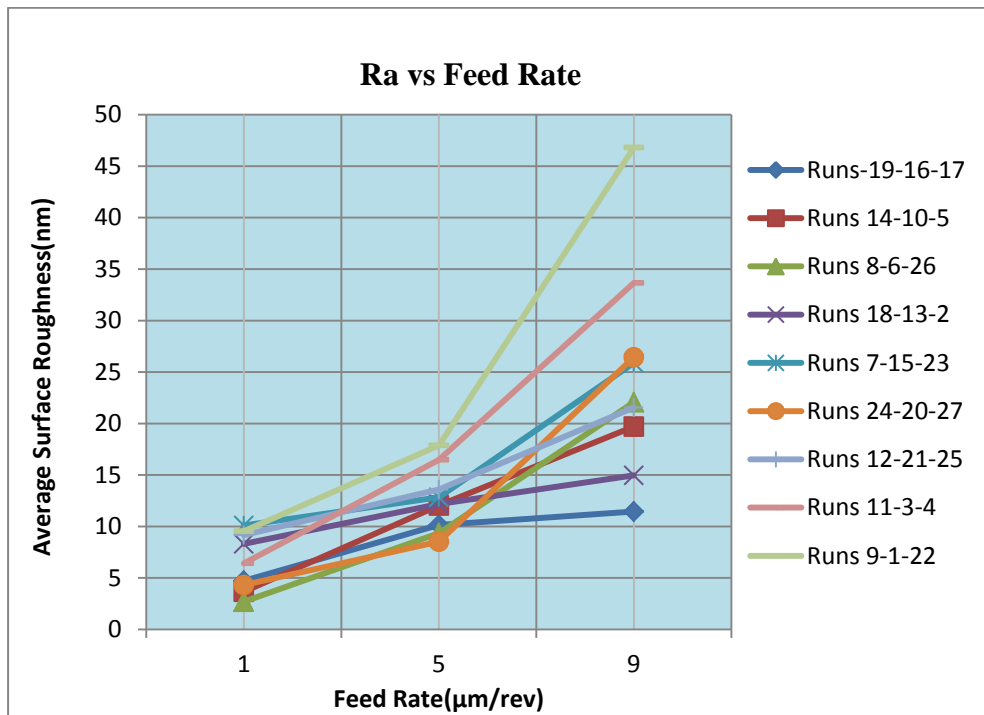


Figure 4.2 The change of average surface roughness with feed rate for 27-runs testing experiment

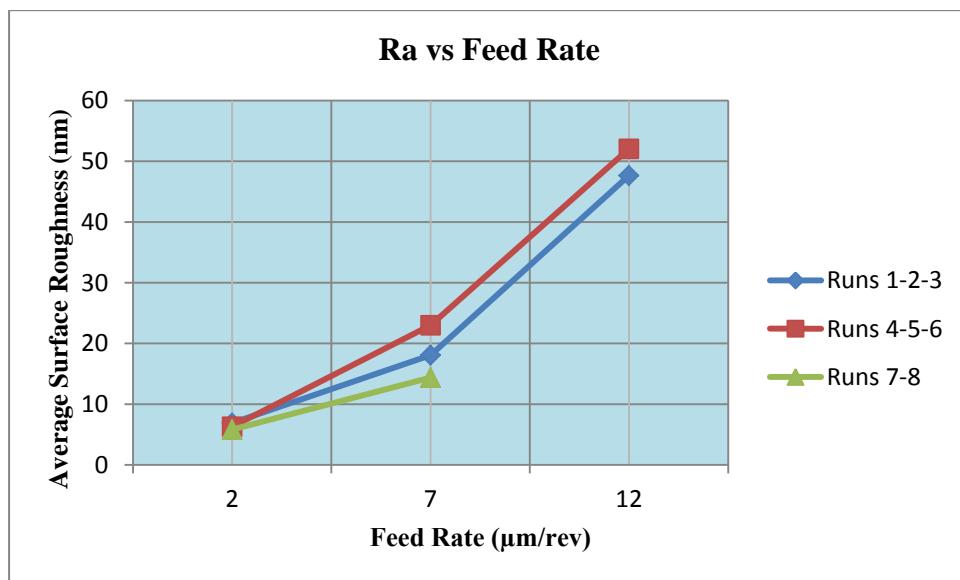


Figure 4.3 The change of average surface roughness with feed rate for 8-runs validation experiment

4.3 Effect of Depth of Cut

The effect of depth of cut is also analyzed during experiments. According to F-test which is conducted by JMP and tabulated in Table 3-11, depth of cut is the second important parameter for surface roughness. Leverage plot also shows that surface roughness values get bigger while the depth of cut increases. Figure 4.4 illustrates the distribution of average surface roughness for different cutting depths and means of the surface roughness for different depth of cuts are tabulated in Table 4-2.

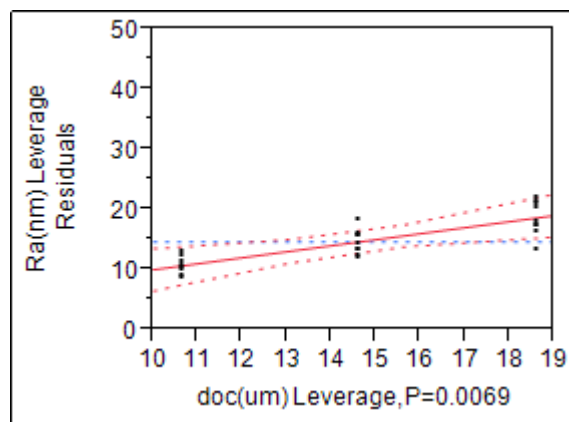


Figure 4.4 Leverage plot for depth of cut

Table 4-2 Least Squares Means Table for depth of cut

Level	Least Sq Mean	Std Error	Mean
22.5	14.58222	1.265647	14.5822
40	18.59778	1.265647	18.5978
5	10.64456	1.265647	10.6446

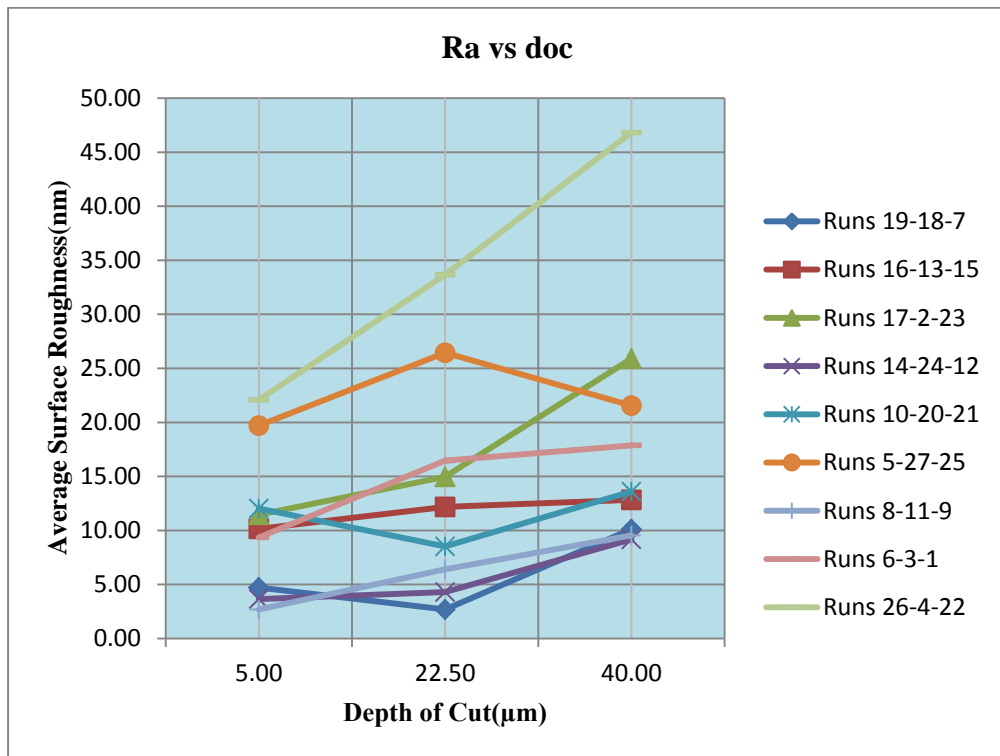


Figure 4.5 The change of average surface roughness with depth of cut for 27-runs experiment

From Figure 4.5, it can not be concluded that there is a simple, linear relationship between surface roughness and depth of cut. However, Table 4-2 shows that there is a trend as; decrease in depth of cut results in lower surface roughness values. Therefore, small depth of cut is advisable during finish turning of PC.

4.4 Effect of Spindle Speed

Spindle speed was the another controlled parameter during this study. Depending on the effect test results, spindle speed turned out to be the least important parameter when compared to feed rate and depth of cut. Pearson’s correlation test also indicated that the effect of spindle speed on surface roughness is not as dominant as feed rate. Figure 4.6 shows that the change of average surface roughness with spindle speed for constant feed rate and depth of cut.

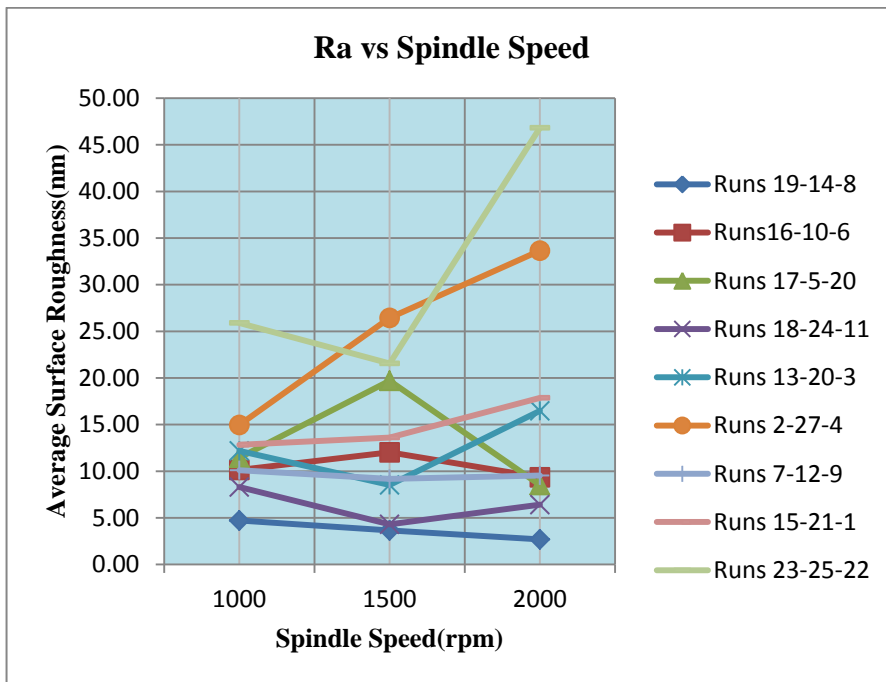


Figure 4.6 The change of average surface roughness with spindle speed for constant feed rate and depth of cut

On the other hand, leverage plot by JMP analysis in Figure 4.7, also shows the distribution of surface roughness with different spindle speeds. Tabulated results for the means of the average surface roughnesses for each spindle speed is given in Table 4-3.

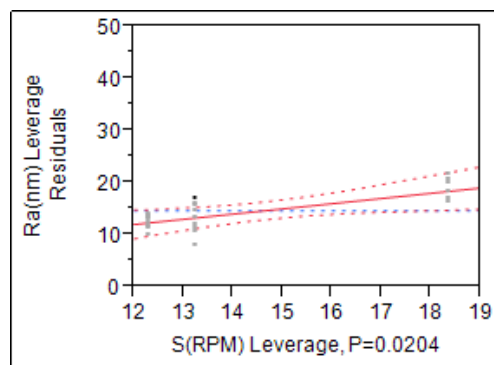


Figure 4.7 Leverage plot for spindle speed

Table 4-3 Least Squares Means Table for spindle speed

Level	Least Sq Mean	Std Error	Mean
1000	12.28667	1.265647	12.2867
1500	13.21911	1.265647	13.2191
2000	18.31878	1.265647	18.3188

Again, there is a tendency for lower surface roughness when the spindle speed decreases. However, the mean of the average surface roughness is not changed drastically between 1000 rpm and 2000 rpm. Therefore, it can be concluded that a significant relation was not observed between spindle speed and surface roughness in that spindle speed range.

4.5 Effect of Vibration

The effect of vibration on surface roughness is investigated by the help of vibration data collection setup which is described in Chapter 3. Vibration signals in x,y, and z directions are gathered for each run. Figure 4.8 illustrates the fast Fourier transform analysis results for the 4th run. All data has been analyzed by Pulse 16.0 software and the rms magnitudes of all signals have been calculated by the software. Then, vibration data in all three directions is examined by SPSS Statistics 20 and Pearson's correlation for vibration has been obtained. In that analysis, V_x , V_y , and V_z all appeared to have higher correlation than depth of cut and spindle speed. Vibration was the second significant factor following the feed rate. Also, the ANN model gave better predictions with the additional vibration information.

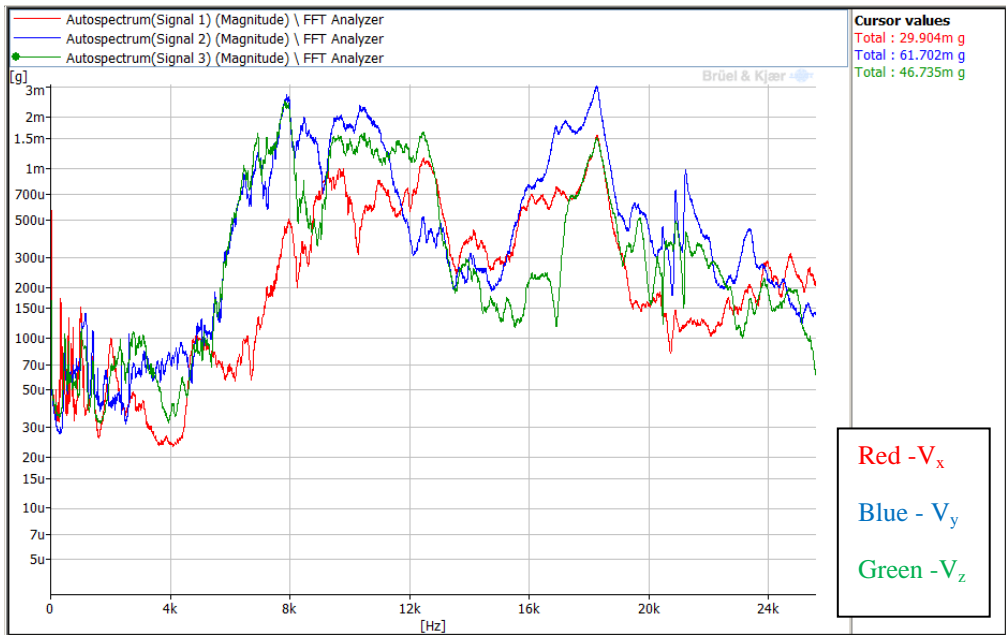


Figure 4.8 Frequency response for 4th run in 27-runs experiment

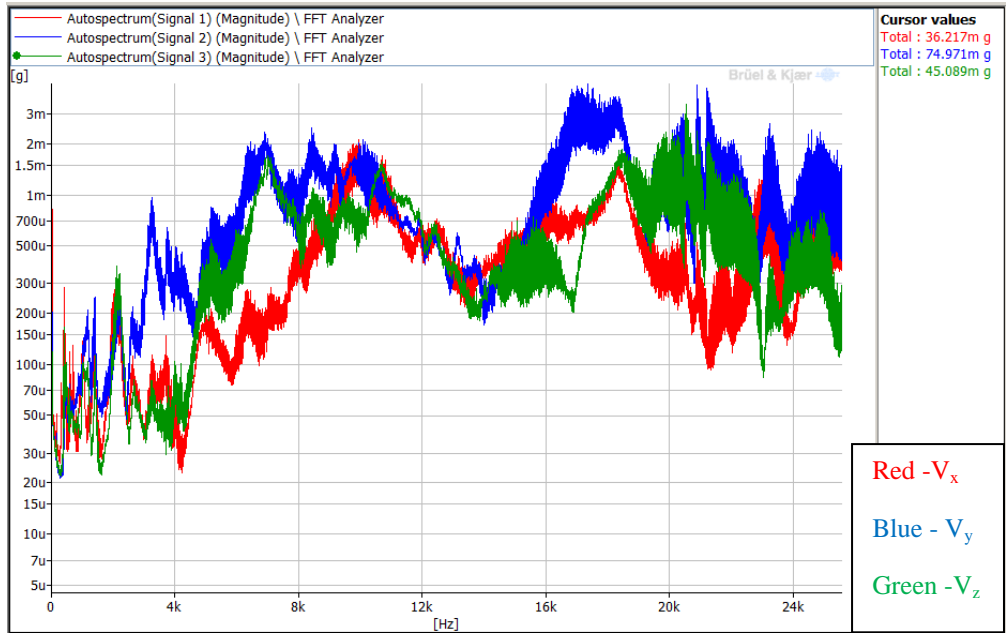


Figure 4.9 Frequency response for 22th run in 27-runs experiment

Analyzing the frequency responses of random runs, Figure 4.8 and Figure 4.9 can provide valuable information about the relation between surface roughness and vibration. Since the vibration amplitudes in all directions are very high in both cases when compared to other vibration data, the average roughness value for these runs were 33.7 and 46.8 nm as the two worst surface quality during 27-runs experiment. These results show that the increase in the magnitude of vibration generally results in very high surface roughness values. However, it does not imply that low vibration values result in good surface quality since 26th run which has one of the lowest vibration data, has a surface roughness value as 22.1 nm. In this run, feed rate with 9 μ m/rev was the dominant factor to determine the surface quality. Therefore, it can be concluded that vibration is a significant factor to determine surface quality but feed rate is more dominant than vibration during finish turning of PC.

For a deeper understanding of the machining process, change of vibration during cutting with same parameters should be further analyzed. As stated in Chapter 2, the crystalline structure of the material could affect the vibration level during machining.

CHAPTER 5

DISCUSSION AND CONCLUSION

In this thesis, finish cutting conditions of PC with a monocrystalline diamond tool are investigated. The effect of feed rate, depth of cut, spindle speed, and vibration on surface roughness of machined PC specimens is experimentally investigated. Feed rate is found as the most dominant factor during finish turning of PC; and vibration, depth of cut and spindle speed have followed, respectively. Three-level full factorial design and ANN model have been used to observe the influence of process parameters and predict the surface roughness.

Flat PC specimens having 30 mm diameter are cut and surface roughnesses of these parts are measured. The best average surface finish is achieved as 2.7 nm and this surface quality level is much below the acceptable average surface roughness level of 25 nm which is determined by SPI A-1 specification of the Society for the Plastic Industry. On the other hand, in the literature the smallest average surface roughness reported was 9 nm, thus the average surface roughness achieved in this study is the smallest. In Table 2-1, the previous studies for PC turning is collected. Although the similar selections for rake angle, clearance angle and tool nose radius have been observed and different machining parameters and machine setup appears to affect the results.

During the experiments, the effect of feed rate, depth of cut and spindle speed are observed while other parameters namely rake angle, clearance angle, properties and application of cutting method are not changed.. Vibration data is also gathered for all runs. Based on these results, ANN modeling and 3-level full factorial design are used to predict the surface roughness and analyze the significance of parameters. The effect of parameters was clarified according to ANOVA and SPSS analysis.

It is highly recommended that feed rate less than $2\mu\text{m}/\text{rev}$, depth of cut less than $5\mu\text{m}$ and spindle speed less than 2000 rpm are to be chosen as cutting parameters in order to obtain high quality PC surfaces having average surface roughness below 5 nm. During cutting process, vibration should be kept as low as possible by stiffening the machine and controlling external disturbances.

5.1 Future Work

During experiments, tool parameters like rake angle and clearance angle are not changed. Effects of these parameters can also be analyzed to obtain optimum surface quality. Pressurized cutting fluid (kerosene) is used during all experiments. Dry cutting conditions can also be examined for finish turning of PC. Different cutting fluids in different pressures can also be tried and its effect on vibration can be experimented. Air cooling can also be tried to see the effect on chip process. Temperature variation can also be analyzed during cutting and temperature values gathered during experiment can add to the ANN model to predict surface roughness in a more accurate way.

In optical industry, acrylic is also used for similar purposes like PC. Therefore, a comparison between them can be made for reaching the best surface quality and performance. The effect of cutting parameters and vibration can be tested on similar materials which have common area of utilization.

Since the vibration on tool holder is significant for the cutting process, an effective vibration control system can be designed by analyzing the data reading from accelerometer. This data can be processed in some control loop algorithm and tool holder position can be controlled with a special tool holder design. As a result, the effect of vibration on surface quality can be minimized.

An accelerometer which is placed on workpiece can give extra information about the effect of vibration change on the surface roughness. PC specimen can be fixed into the chuck to eliminate the vibration due to centering.

Alternative diamond tools (e.g. polycrystalline) can also be tried for finish cutting of PC so that the cost of production can be minimized without sacrificing surface quality. In this study, wear of diamond tools is not analyzed. On the contrary to common belief that wear is not an important problem during cutting plastics, it may cause serious problems on surface quality as explained in Chapter 2. Therefore, tool wear inspection may be an important phenomenon during machining of plastics.

REFERENCES

1. <http://www.aselsan.com/content.aspx?mid=375&oid=458>, Aselsan Inc., last accessed on 10 May 2013.
2. <http://clancyoptical.net/lens-materials/>, Clancy Optical & Spex Eyewear, last accessed on 10 March 2013.
3. Alauddin, M., et al., "Plastics and their machining: A review", *Journal of Materials Processing Technology*, 1995. 54(1-4): p. 40-46.
4. Li, L., J.S.A. Collins, and A.Y. Yi, "Optical Effects of Surface Finish by Ultraprecision Single Point Diamond Machining", *Journal of Manufacturing Science and Engineering*, 2010.
5. Gubbels, G., "Diamond Turning of Glassy Polymers, Technische Universiteit Eindhoven, 2006.
6. J.M. Elson, J.P.R., and J.M. Bennett., "Relationship of the total integrated scattering from multilayer-coated optics to angle of incidence, polarization, correlation length, and roughness cross-correlation properties", *Applied Optics*, 22(20):3207-3219, 1983.
7. Riedl, M., "Advances in single-point diamond turning provide improved performance for visible as well as ir optics". SPIE's OE-magazine, 2004.
8. <http://eckop.com/optics/understanding-your-optical-engineer/optical-scattering-versus-surface-roughness/>, Eckhardt Optics LLC, last accessed on 14 April 2013.
9. Hecht, E., "Optics", 2nd ed. 1987, Massachusetts: Addison-Wesley Publishing Company.
10. Fetecau, C., et al., "Machining and surface integrity of polymeric materials", *International Journal of Material Forming*, p. 515-518, 2008
11. Drescher, J.D., "Tool Force, Tool Edge, and Surface Finish Relationships in Diamond Turning", North Carolina State University, 1991
12. Smith, E.F., "Single-point diamond turning of amorphous thermoplastic polymers", Master's thesis, North Carolina State University, Raleigh, NC, 1989.
13. Arcona, C., "Tool force, chip formation and surface finish in diamond turning", PhD thesis, North Carolina State University, Raleigh, 1996.
14. Gubbels, G., et al., "Diamond tool wear when cutting amorphous polymers", *CIRP Annals - Manufacturing Technology*, Vol. 53(2004), p. 447-450, 2004.

15. Horne, D.F., "Optical Production Technology", 2nd ed. 1983, Briston, Adam Hilger Ltd.
16. Evans, C.J., "Precision engineering: an evolutionary perspective", *Philosophical Transactions of the Royal Society, Mathematical, Physical and Engineering Sciences*, p. 3835-3851, 2012
17. Benjamin, R.J., "Diamond Turning at a Large Optical Manufacturer", *Optical Engineering*, p. 176574-176574, 1978.
18. Venkatesh, V.C. and S. Izman, "Precision Engineering", 2007: Tata McGraw-Hill Publishing Company Limited.
19. V.K.Saini, et al. "Optimisation of process parameter in ultra-precision diamond turning of polycarbonate material", *Proceedings of the International Conference on Manufacturing Excellence MANFEX 2012*. Amity University Campus, Noida (UP), INDIA.
20. Carr, J.W. and C. Feger, "Ultraprecision machining of polymers", *Precision Engineering*, p. 221-237, 1993.
21. Yergök, Ç., "Rough cutting of germanium with polycrystalline diamond tools", Master of Science Thesis, Mechanical Engineering Department, Middle East Technical University, Ankara, 2010.
22. Gubbels, G.P.H., Beek, G.J.F.T. van der, Delbressine, F.L.M. & Schellekens, P.H.J. (2004), "Electrostatic tool wear in diamond turning of amorphous polymers", *Proceedings of the 4th Euspen International Conference*, (pp. 97-98). United Kingdom, Glasgow.
23. Evans, C., 1991, "Cryogenic diamond turning of stainless steel", *Annals of the CIRP*, 40/1:571-575.
24. Paul E., Evans C.J., Mangamelli A., McGlaufflin M.L., Polvani R.S., "Chemical aspects of tool wear in single point diamond turning", *Precision Engineering*, 1996.
25. R. Wada, H. Kodama, K. Nakamura, Y. Mizutani, Y. Shimura, N. Takenaka, "Wear characteristics of single crystal diamond tool", *Ann. CIRP* 29 (1) (1980) 47–52.
26. Shi, M., et al., "Diamond tool wear measurement by electron-beam-induced deposition", *Precision Engineering*, p. 718-721, 2010.
27. Kopač, J. and S. Šali, "Tool wear monitoring during the turning process", *Journal of Materials Processing Technology*, p. 312-316, 2001.
28. Cheung, C., "Modelling and simulation of nano-surface generation in ultra-precision machining", The Hong Kong Polytechnic University, 2000.

29. Jasinevicius, R.G., et al., "Critical aspects on the behavior of material from the mechanical tool-workpiece interaction in single point diamond turning", *Journal of the Brazilian Society of Mechanical Sciences*, p. 509-518, 1999.
30. Lee, W.B., To, S., Cheung, C.F., "Effect of crystallographic orientation in diamond turning of copper single crystals", *Scripta Materialia*, Vol 42, pp. 937-945. (2000).
31. Xiao, K.Q. and L.C. Zhang, "The role of viscous deformation in the machining of polymers", *International Journal of Mechanical Sciences*, 2002. 44(11): p. 2317-2336.
32. Aydın, M., et al., "Prediction of surface roughness and cutting zone temperature in dry turning processes of AISI304 stainless steel using ANFIS with PSO learning", *The International Journal of Advanced Manufacturing Technology*, 2013. 67(1-4): p. 957-967.
33. Kamruzzaman, M. and Dhar, N. R., "An Experimental Investigation into Tool Wear, Tool Life and Product Quality in Turning Steel under High-Pressure Coolant Condition", *Proceedings of the Global Conference on Production and Industrial Engineering (CPIE-2007)*, Jalandhar, India.
34. Jin Li Wang et al., 2011, "Advanced Materials Research", 189-193, 3187.
35. E. Trent, and Wright, P.K, "Metal cutting fourth edition", Butterworth-Heinemann, Boston, M.A, 2000.
36. Chen, C., et al., "Experimental investigation of tool vibration and surface roughness in the precision end-milling process using the singular spectrum analysis", *The International Journal of Advanced Manufacturing Technology*, 2012. 63(5-8): p. 797-815.
37. Thomas, M., et al., "Effect of tool vibrations on surface roughness during lathe dry turning process", *Computers & Industrial Engineering*, 1996. 31(3-4): p. 637-644.
38. İ.Asiltürk, "On-line surface roughness recognition system by vibration monitoring in CNC turning using adaptive neuro-fuzzy inference system (ANFIS)", *Int. Journal of Physical Sciences*, Volume 6 (22), 2011, pp. 5353-5360.
39. Sohn, A., L. Lamonds, and K. Garrard, "Modeling of Vibration in Single Point Diamond Turning", North Carolina State University: Raleigh, North Carolina, USA.
40. Abuthakeer, S.S., P.V. Mohanram, and G. Mohankumar, "The Effect of Spindle Vibration on Surface Roughness of Workpiece in Dry Turning Using Ann", *International Journal of Lean Thinking*, 2011. 2(2): p. 42-58.
41. W. B. Lee, C. F. Cheung et al., "Materials Induced Vibration in Ultra-Precision Machining", *J. of Materials Processing Technology*, 89-90, pp. 318-325, 1999.

42. Chen, C.-C. and K.-T. Chiang, "Analyzing the design of vibration reduction with the rubber-layered laminates in the precision turning with a diamond cutting tool", *The International Journal of Advanced Manufacturing Technology*, 2011. 57(1-4): p. 101-116.
43. Kyun Baek, D., T. Jo Ko, and H. Sool Kim, "A dynamic surface roughness model for face milling", *Precision Engineering*, 1997. 20(3): p. 171-178.
44. Kassab S. Y. and Khoshnaw Y. K., (2007), "The Effect of Cutting Tool Vibration on Surface Roughness of Work piece in Dry Turning Operation", *Engineering and Technology*, Volume 25, Number 7, pp. 879-889.
45. Armarego, E.J.A. and Whitfield, R.C., "Computer based modeling of popular machining operations for force and power predictions", *Annals of the CIRP* , 34: 65-69), 1985.
46. Dimla D. E. Snr., "The correlation of vibration signal features to cutting tool wear in a metal turning operation", *International Journal of Advanced Manufacturing*, 2000, 19(10), 705-713.
47. Özel T, Karpat Y., "Predictive modeling of surface roughness and tool wear in hard turning using regression and neural networks, *Int. J. Mach. Tools Man.*, 45(4-5): 467-479, 2005.
48. Çalı, S, "An Experimental Study on Single Crystal Diamond Turning of Optical Quality Silicon", Master of Science Thesis, Mechanical Engineering Department, Middle East Technical University, Ankara, 2008.
49. Aslan E, Camuscu N, Birgoren B (2007), "Design optimization of cutting parameters when turning hardened AISI4140 steel with AL2O3 + TiCN mixed ceramic tool", *Materials and Design* 28:1618-1622.
50. A.M.A. Al-Ahmari, "Predictive machinability models for a selected hard material in turning operations", *Journal of Materials Processing Technology* Volume 190, Issues 1– 3, Pages 305–311, 2007.
51. Janez Kopac, Marko Bahor and Mirko Sokovic, " Optimal machining parameters for achieving the desired surface roughness in fine turning of cold pre-formed steel workpieces ", *International Journal of Machine Tools & Manufacture*, Vol.42, pp.707-716, 2002.
52. Huang, L. and Chen, J., "A multiple regression model to predict in-process surface roughness in turning operation via accelerometer", *Journal of Industrial Technology*, pp. 1-8, 2001
53. Xu, H., et al., "Study on the control of surface roughness in single point diamond turning", p. 84161D-84161D, 2012.

54. Khatri, N., V. Mishra, and R.G.V. Sarepaka, "Optimization of Process Parameters to Achieve Nano Level Surface Quality on Polycarbonate" International Journal of Computer Applications. 48(13): p. 39-44.
55. Singh, H., et al., "Analysis of Surface Roughness and Waviness During Diamond Turning of Polycarbonate", International Journal of Scientific Research, 2013.
56. Goupy, J., Creighton, L., "Introduction to Design of Experiments with JMP® Examples", Cary, Third Edition, SAS Institute Inc., 2007.
57. <http://www.itl.nist.gov>, National Institute of Standards and Technology, last accessed on 28 March 2013.
58. Karow, K.H., "Fabrication Methods for Precision Optics", John Wiley & Sons, Inc., 1993.
59. Asiltürk, İ., "Application of Artificial Intelligent to Predict Surface Roughness", Experimental Techniques, 2012.
60. Nalbant, M., H. Gokkaya, and I. Toktas, "Comparison of regression and artificial neural network models for surface roughness prediction with the cutting parameters in CNC turning", Model. Simul. Eng., 2007. 2007(2): p. 1-14.
61. NASA, "Precision Diamond Turning of Aerospace Optical Systems", Practice No. PD-ED-1265.
62. Schaefer, J., Scott, S., "Single Point Diamond Turning of Optical Components", Texas Instruments Incorporated, Custom Optics Services, 1991.
63. www.contour-diamonds.com, Contour Fine Tooling, last accessed on 8 April 2013.
64. <http://www.plastics.bayer.com/landingpages/makrolon-com.aspx>, BAYER MaterialScience AG, last accessed on 2 July 2013.
65. <http://www.hermlemachine.com/>, HERMLE Machine Company, last accessed on 23 November 2012.
66. Bennett, J.M., et al., "Standards For Optical Surface Quality Using Total Integrated Scattering", p. 124-132, 1979.
67. T.V.Vorburger, J.Raja., "Surface Finish Metrology Tutorial", June 1990.
68. Srivatsan, T.S., "A review of: FUNDAMENTALS OF MACHINING AND MACHINE TOOLS by Goeffrey Boothroyd and Winston A", Knight Marcel Dekker, Inc., New York Second edition, 542 pages, hardcover, 1989. Materials and Manufacturing Processes, p. 485-487, 1990.
69. <http://www.micromanufacturing.com/content/understanding-scanning-white-light-interferometry>, MICRO manufacturing, last accessed on 3 January 2013.

70. www.zygo.com, Zygo Corporation, last accessed on 28 March 2013.
71. <http://www.mitsubishicarbide.net>, Mitsubishi Material, last accessed on 7 March 2013.

APPENDIX A

SURFACE ROUGHNESS PARAMETERS

R_a is the arithmetic mean of the absolute values. It is calculated as in Equation (A.1) and R_a roughness measurement of the machined surface is shown in Figure A.1 [21].

$$R_a = 1/Q \int_0^Q \{z(x)\} dx \quad (A.1)$$

Where;

R_a : Arithmetic Surface Roughness

Q : Sampling length

$z(x)$: Roughness curve

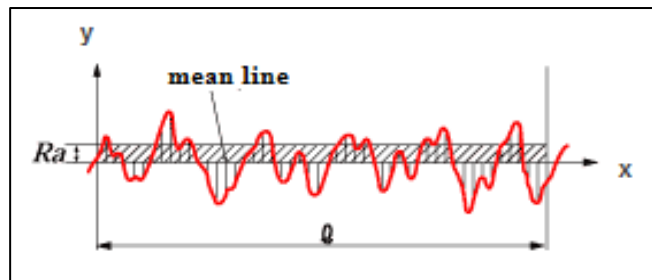


Figure A.1 R_a Roughness Measurement [71]

R_q or rms is the root mean square measurement of the surface roughness and it is calculated as in the Equation (A.2). Figure A.2 shows the R_q or rms roughness measurement of the machined surface [21].

$$R_q = \sqrt{1/Q \int_0^Q \{z^2(x)\} dx} \quad (A.2)$$

Where;

R_q : Root Mean Square Roughness

Q : length of the surface

$z(x)$: Roughness curve

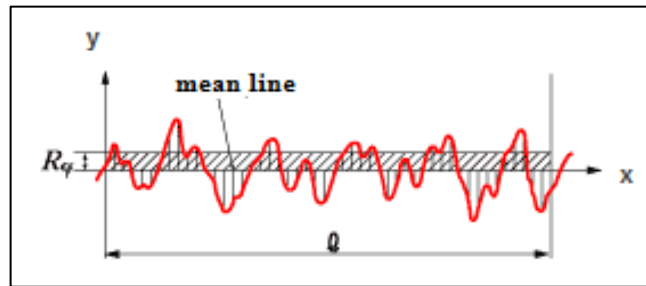


Figure A.2 R_q or rms Roughness Measurement [71]

R_z or PV is the sum of R_p and R_v where R_p is the top peak height and R_v is bottom valley depth on the surface. R_z or PV (Peak to Valley) roughness of the surface is shown in Figure A.3 [21].

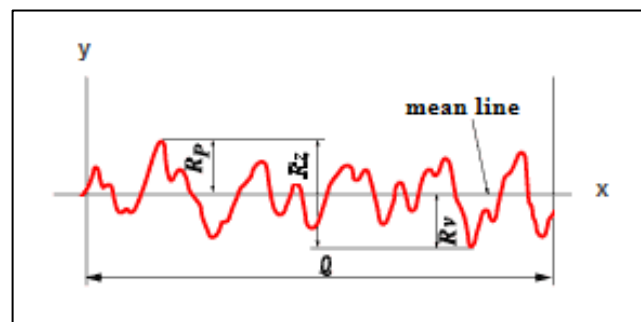


Figure A.3 R_z or PV Roughness Measurement [71]

APPENDIX B

TECHNICAL SPECIFICATIONS OF SINGLE POINT DIAMOND TURNING MACHINE

Table B-1 Technical Specifications of Pretitech Freeform 700U [21]

Machine Property	Description
Base	Sealed natural granite base
Type	Ultra-precision, two, three or four axes CNC contouring machine
Programming Resolution	0.01 nm linear, 0.0000001° rotary
Slideways Position Feedback Resolution	0.032 nm
Slideways X-axis Straightness	Horizontal: 0.30 μm full travel
Slideways Z-axis Straightness	Horizontal: 0.40 μm full travel
Slideways Vertical Straightness	X: 0.75 μm, Z: 0.75 μm
Vibration Isolation	Self leveling dual chamber pneumatic isolation system
Drive System	AC linear motor
Swing Capacity	700 mm
Slide Travel	X- 350 mm, Z- 300 mm
Maximum Feed Rate	4000 mm/min
Workholding Spindle Air Bearing Type	Slot-type thrust bearing
Workholding Spindle Motor	Integral brushless motor
Workholding Spindle Load Capacity	68 kg
Workholding Spindle Maximum Speed	7000 RPM
Workholding Spindle Axial Stiffness	228 N/μm
Workholding Spindle Radial Stiffness	88 N/μm
Workholding Spindle Motion Accuracy	Axial/Radial ≤ 25 nm
Thermal Control	Liquid cooled chiller ± 0.1 °C accuracy
C-axis Feedback Resolution	0.026 arc-sec
C-axis Position Accuracy	± 2 arc-sec
C-axis Maximum Speed	3000 RPM
B-axis Tabletop Size	380 mm
B-axis Load Capacity	454 kg
B-axis Maximum Speed	10 RPM
B-axis Position Feedback Resolution	0.003 arc-sec
B-axis Radial Stiffness	525 N/μm
B-axis Axial Stiffness	875 N/μm

APPENDIX C

TOOL NUMBERING SYSTEM OF CONTOUR FINE TOOLING COMPANY

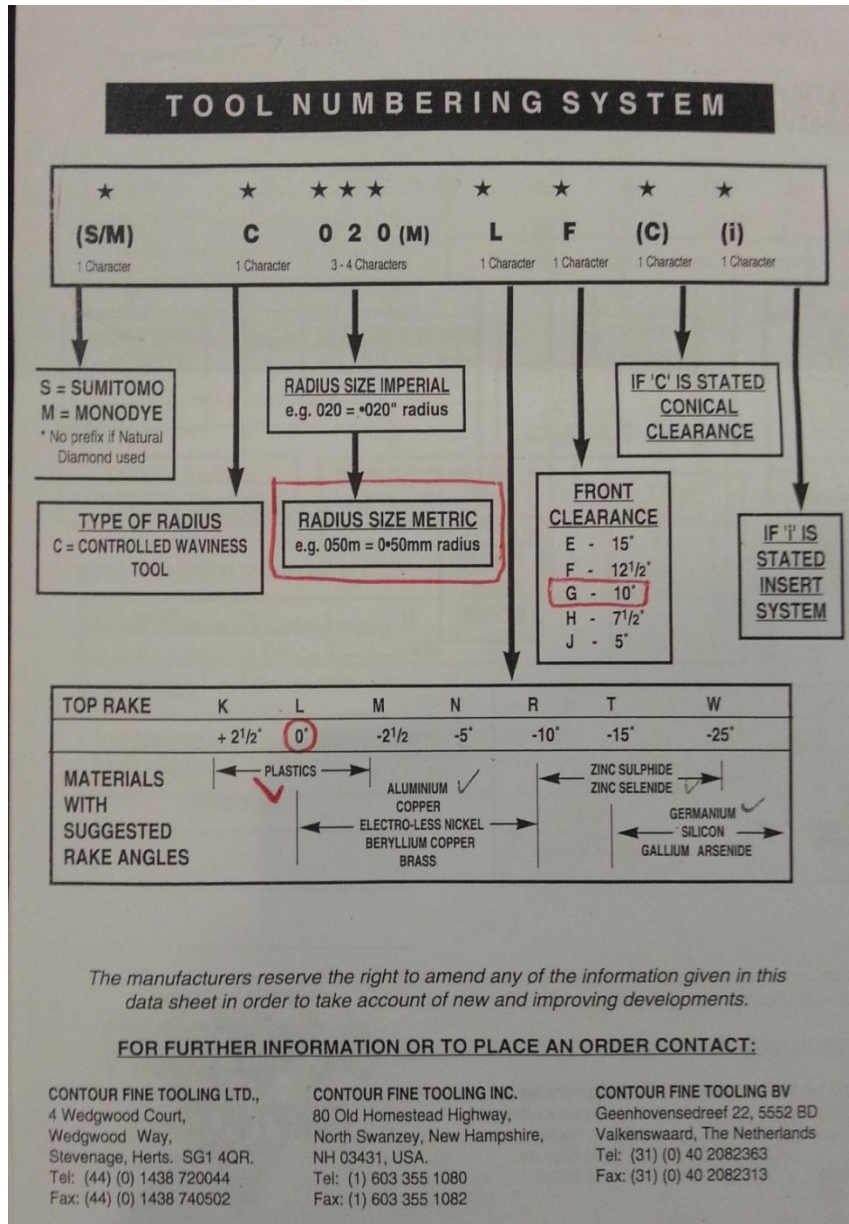


Figure C.1 Tool Numbering System for Monocrystalline Diamond Tool

APPENDIX D

PRODUCT DATA SHEET FOR POLYCARBONATE



Product Data Sheet, July 2012

Makrolon® UV

Solid polycarbonate sheet



Your benefits:

- excellent weathering resistance
- extreme impact strength
- good fire rating
- thermoformable

Makrolon® UV sheets are made from clear-transparent polycarbonate sheets with UV protection on both sides. They are the perfect choice for a long service life owing to their good weathering resistance. These attributes are backed up by our 10-year guarantee on weathering resistance and a 10-year guarantee on retaining their mechanical properties.

Applications:
Makrolon® UV is ideal for outdoor applications:

- covered walkways and bus shelters
- barrel vaults and skylights (also thermoformed)

Available sizes:
Makrolon® UV is available in thicknesses of 2 – 15 mm and in the following sizes; other sizes, colors and sheet thicknesses on request.

Colors:	Sizes (Standard):
clear 2099	2,050 x 1,250 mm
white 2190	3,050 x 2,050 mm
white 2150	6,110 x 2,050 mm
bronze 2860	
gray 2700	
blue 2550	
green 2650	

	Test Conditions	Typical value ⁽¹⁾	Unit	Standard
PHYSICAL				
Density	water at 20 °C	1.200	g/cm ³	ISO 1183-1
Water absorption saturation	23 °C, 90% relative humidity	0.30	%	ISO 62
Water absorption equilibrium	23 °C, 90% relative humidity	0.12	%	ISO 62
Refractive index	Procedure A	1.897	-	ISO 688
MECHANICAL				
Impact modulus	1 mm/min	2300	MPa	ISO 627-1, -2
Yield stress	80 mm/min	120	MPa	ISO 627-1, -2
Yield strain	80 mm/min	0	%	ISO 627-1, -2
Nominal strain at break	80 mm/min	1.80	%	ISO 627-1, -2
Flexural modulus	2 mm/min	2300	MPa	ISO 178
Flexural strength	2 mm/min	90	MPa	ISO 178
Charpy impact strength	23 °C, unnotched	non-break	kJ/m ²	ISO 179-1&2
Charpy impact strength	23 °C, 2 mm	800	kJ/m ²	ISO 179-1&2
Izod impact strength	23 °C, 2.5 mm, notched	800	kJ/m ²	ISO 180-A
THERMAL				
Heat softening temperature	80 Hz, 50°C/h	148	°C	ISO 302
Thermal conductivity	23°C	0.20	W/m·K	ISO 8502
Coefficient of linear thermal expansion	25 to 235°C	0.68	10 ⁻⁶ /K	ISO 11359-1, -2
Temperature of deflection under load	1.80 MPa	128	°C	ISO 11359-1, -2
Temperature of deflection under load	0.45 MPa	140	°C	ISO 11359-1, -2
ELECTRICAL				
Electrical strength	1 mm	35	kV/mm	IEC 60243-1
Volume resistivity		1E12	Ohm·m	IEC 60243
Surface resistivity		1E12	Ohm	IEC 60243
Relative permittivity	100 Hz	3.1	-	IEC 60243
Relative permittivity	1 MHz	3.0	-	IEC 60243
Dielectric factor	100 Hz	8	10 ⁻⁴	IEC 60243
Dielectric factor	1 MHz	88	10 ⁻⁴	IEC 60243

⁽¹⁾ These values are measured on injection molded samples, and are not intended for specification purposes.

Product Liability Clause: This information and our technical advice – whether verbal, in writing or by way of this – are given in good faith but without warranty, and this also applies where proprietary rights of third parties are involved. Our advice does not release you from the obligation to verify the information currently provided – especially that contained in our safety data and technical information sheets – and to test products as to their suitability for the intended processes and uses. The application, use and processing of our products and the products manufactured by you on the basis of our technical advice are beyond our control and, therefore, entirely your own responsibility. Our products are sold in accordance with the current version of our General Conditions of Sale and Delivery.

Makrolon® is a registered trademark of Bayer AG

NF 0112 8


makrolon®
UV

Figure D.1 Product Data Sheet for Polycarbonate

Product Data Sheet, July 2012

Makrolon® UV

Solid polycarbonate sheet



Bayer MaterialScience S-Line, the standard product line, represents a range of certified quality products which offer the reliable solution for most applications.

Light Transmission: Test Method according to DIN 5036

The stated thicknesses are not all available as standard. Please ask us for more information. The stated values are typical values only.

Light transmission in %	2	3	4	5	6	8	10	12	15
Makrolon® UV clear 2020	88	87	87	86	85	84	82	81	79
Makrolon® UV white 2150	49	50	53	16	13				
Makrolon® UV white 2150	60	59	49	33	28	20			
Makrolon® UV bronze 2050	63	59	50	50	50	50	42	36	
Makrolon® UV grey 2700		62	55	49	43	34	28		
Makrolon® UV green 2050		77	73	71	68	62	60	56	
Makrolon® UV blue 2050		61	58	51	46	40			

Fire Rating (°): Oxygen Index (LOI) 25% ISO 4589-2 Method A.

Country	Standard	Rating	Thickness	Color
Germany	DIN 4102	B2	0,75 – 16 mm	all colors
	DIN 9510-2	S2 SR2 ST2	4 mm	white 2150
	DIN 9510-2	S2 SR2 ST2	4 mm	white 2150
UK	BS 476 Part 7	Class 1Y	2,5,4,6 & 12 mm	clear 2020
	BS 476 Part 7	Class 1Y	5 mm	white 2150
France	NF P 92-501&505	M2	2 – 16 mm	clear 2020
		M2	2 – 12 mm	bronze 2050
	NF F 16-101&102	F2	2 – 16 mm	clear 2020
		F2	2 – 12 mm	bronze 2050
Italy	CSE RF 2/75/A	Classo 1	2 – 10 mm roof	all colors
		Classo 1	2 – 6 mm wall	all colors
Europe	EN 13501-1	B s1 d0	1 – 6 mm	clear 2020
		B s1 d0	1 – 3 mm	white 2150

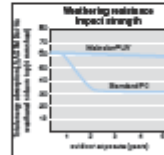
Glow wire flammability index, IEC 60695-2-12, in °C (°):

	2	3	4	5	6
Makrolon® UV clear 2020	900				900
Makrolon® UV bronze 2050		900	900		
Makrolon® UV white 2150	900	900	900		
Makrolon® UV white 2150		900	900	900	900

(*) Fire certificates are listed in time and scope, always check if the mentioned certificate is valid for the purchased Polycarbonate sheet type at the date of delivery. Polycarbonate sheets may change their fire behavior due to aging and weathering. The indicated fire rating was tested on new / unweathered Product in accordance with the indicated fire-classification standards.

Weathering Resistance: Makrolon® UV sheets show excellent weathering resistance, which guarantees their impact strength even after many years. Since their introduction in 1989, the sheets have been examined in an intensive test program, including a real-time outdoor exposure test in a southern European climate (Bando) and in hot and humid regions (Florida and Singapore). The sheets are provided with a 10-year warranty on unbreakability and on optical properties.

Permanent Service Temperature: The permanent service temperature without load is approx. 120 °C.



Bayer MaterialScience

Bayer MaterialScience GmbH
 Otto-Hesse-Straße 19/TF9, 64293 Darmstadt, Germany
 Tel. +49 615113 03-0
 Fax +49 6151 13 03-500

www.bayersheeteurope.com

Figure D.1 (cont'd)

APPENDIX E

TECHNICAL SPECIFICATIONS OF WHITE LIGHT INTERFEROMETRY

Table E-1 Technical Specifications of Zygo NewView 5000 Interferometry

Property	Description
Measurement Technique	Non-contact, 3-D, scanning white-light and optical phase-shifting interferometry
Objectives	Infinite conjugate interferometric objectives; 1X, 2X, 2.5X, 5X, 10X, 20X, 50X, 100X
Measurement Array	Standard, selectable, include: 640x480, 320x240, 160x120
Vertical Resolution	Up to 0.1 nm
Lateral Resolution	0.45 to 11.8 μm , objective dependent
Working Distance	0.55 to 20.5 mm, objective dependent
Focus Depth	± 0.5 to 322.5 μm , objective dependent
Field of View (H x V)	0.070 x 0.053 to 7.00 x 5.30 mm, objective dependent
Maximum Slope	1.41° to 33.25°, objective dependent
Maximum Data Points	307,200; dependent upon sampling array
Test Part Material	Various, opaque and transparent surface; coated and uncoated; specular and nonspecular
Test Part Reflectivity	1-100 %

APPENDIX F

SURFACE ROUGHNESS MEASUREMENTS

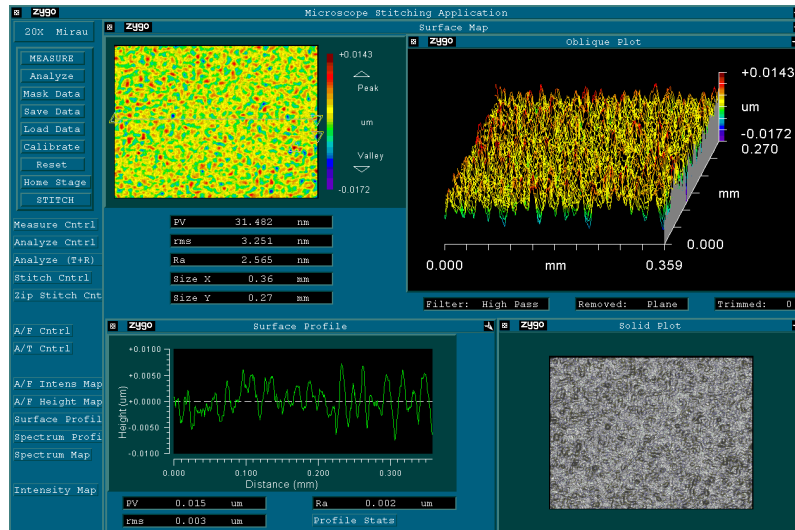


Figure F.1 1st measurement for 8th run of 3^{^3} full factorial design

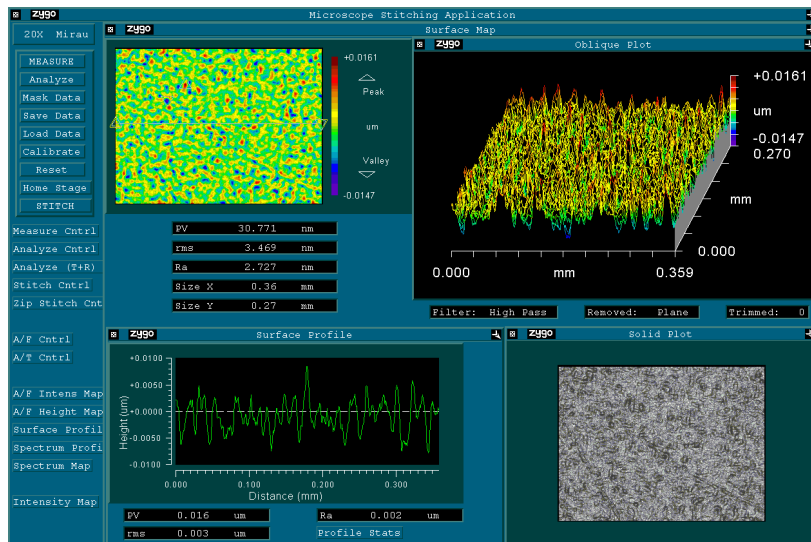


Figure F.2 2nd measurement for 8th run of 3^{^3} full factorial design

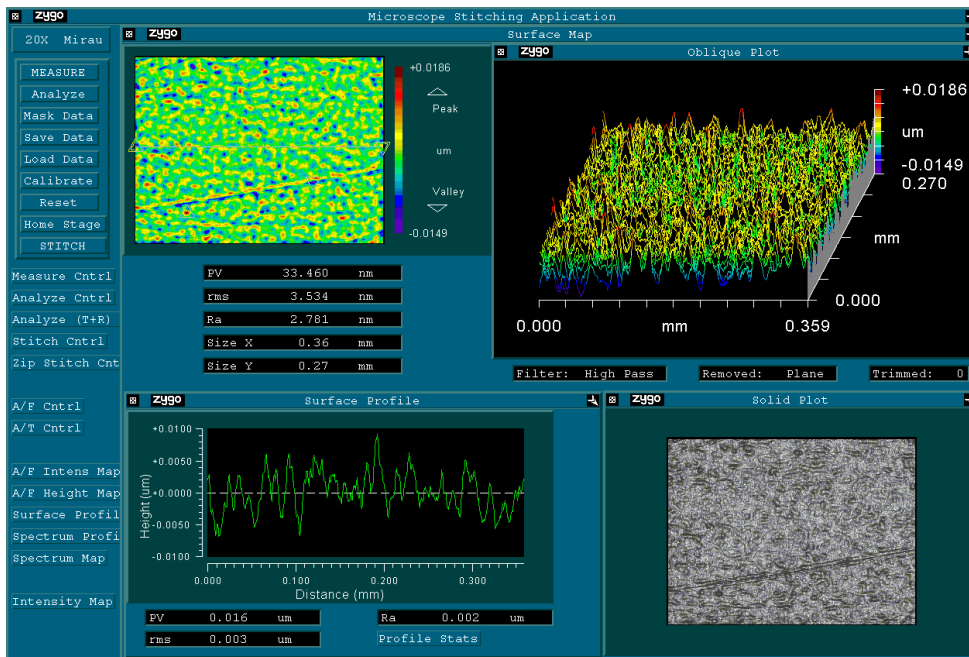


Figure F.3 3rd measurement for 8th run of 3³ full factorial design

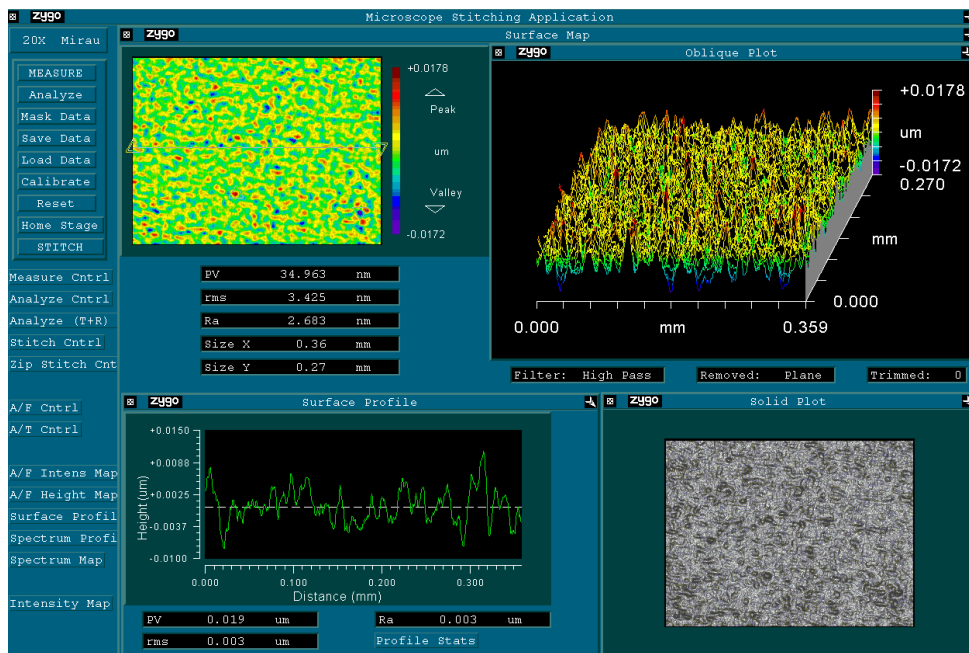


Figure F.4 4th measurement for 8th run of 3³ full factorial design

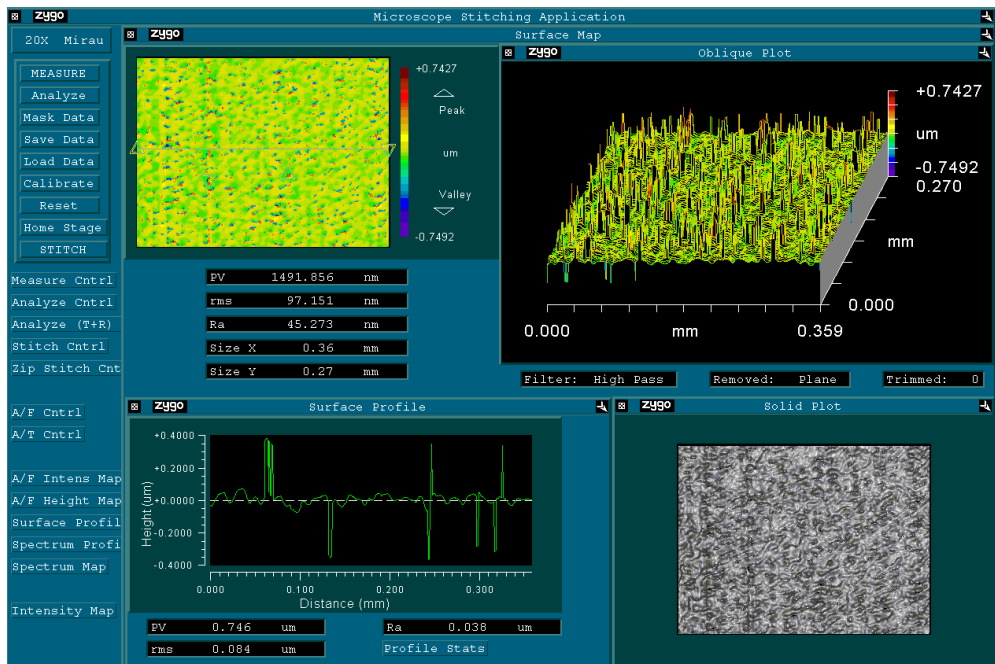


Figure F.5 1st measurement for 22nd run of 3[^]3 full factorial design

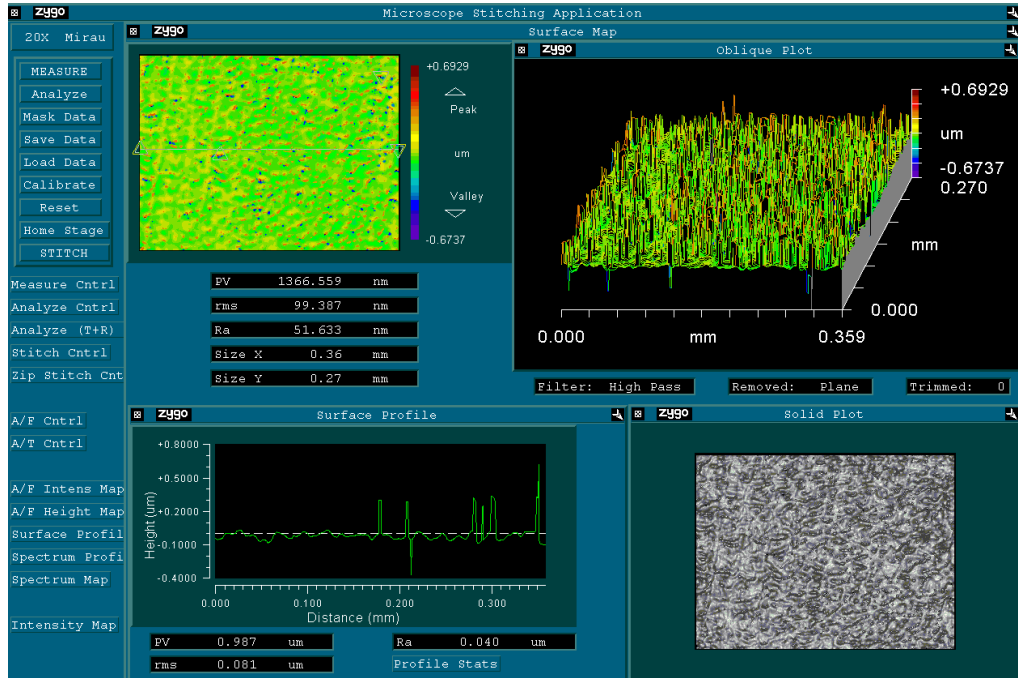


Figure F.6 2nd measurement for 22nd run of 3[^]3 full factorial design

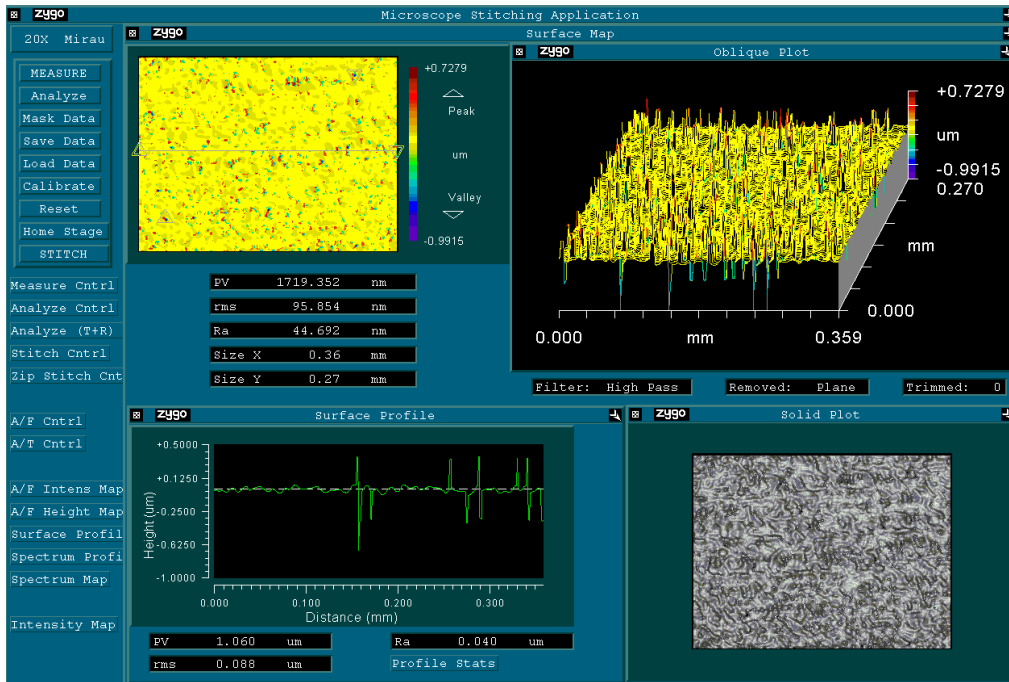


Figure F.7 3rd measurement for 22nd run of 3[^]3 full factorial design

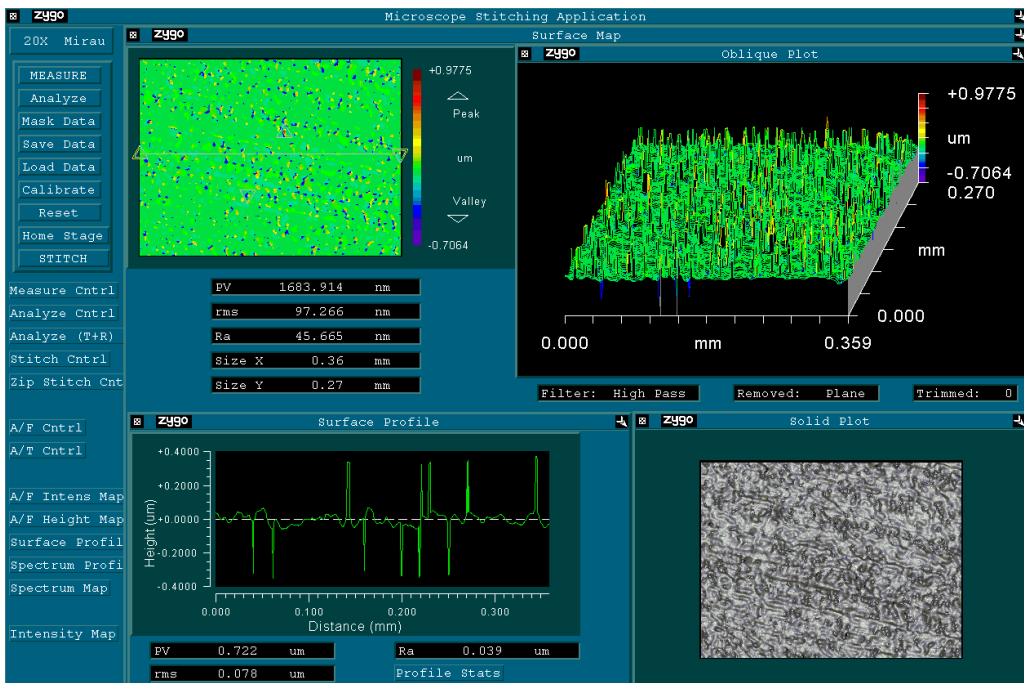


Figure F.8 4th measurement for 22nd run of 3[^]3 full factorial design

APPENDIX G

ALL SURFACE ROUGHNESS MEASUREMENTS FOR 27-RUNS TESTING EXPERIMENT

Table G-1 Surface Roughness measurements for 27-runs testing experiment

Run	Position #	Feed Rate	Depth of Cut	Spindle Speed	Ra	PV	rms
		($\mu\text{m}/\text{rev}$)	(μm)	(RPM)	(nm)	(nm)	(nm)
1	1	5	40	2000	16.8	759.9	25.2
	2				18.7	747.3	30.9
	3				19.0	750.2	30.9
	4				17.0	739.6	23.2
	Average				17.9	749.3	27.5
2	1	9	22.5	1000	13.2	695.9	15.6
	2				14.7	396.0	17.5
	3				15.3	109.0	17.9
	4				16.6	398.9	19.4
	Average				15.0	399.9	17.6
3	1	5	22.5	2000	17.4	712.7	39.2
	2				12.7	694.2	15.5
	3				18.6	434.9	35.3
	4				17.2	425.8	27.0
	Average				16.5	566.9	29.3
4	1	9	22.5	2000	31.1	1057.0	59.8
	2				44.9	1425.7	91.4
	3				31.1	1141.9	60.5
	4				27.6	783.1	44.9
	Average				33.7	1101.9	64.2
5	1	9	5	1500	19.3	463.6	26.9
	2				18.8	759.1	25.0
	3				19.0	737.0	23.9
	4				21.7	758.8	27.5
	Average				19.7	679.6	25.8
6	1	5	5	2000	6.1	69.8	7.7
	2				10.3	669.0	13.3
	3				10.2	693.3	13.1
	4				10.8	744.5	14.3
	Average				9.4	544.2	12.1

Table G-1 (cont'd)

Run	Position #	Feed Rate	Depth of Cut	Spindle Speed	Ra	PV	rms
		($\mu\text{m}/\text{rev}$)	(μm)	(RPM)	(nm)	(nm)	(nm)
7	1	1	40	1000	8.4	81.0	10.7
	2				8.5	410.6	11.4
	3				13.8	103.8	16.8
	4				9.8	467.3	12.5
	Average				10.1	265.7	12.9
8	1	1	5	2000	2.6	31.5	3.3
	2				2.7	30.8	3.5
	3				2.8	33.6	3.5
	4				2.7	35.0	3.4
	Average				2.7	32.7	3.4
9	1	1	40	2000	9.5	115.9	12.0
	2				9.4	107.8	11.9
	3				9.2	104.7	11.6
	4				10.0	275.0	12.6
	Average				9.5	150.8	12.0
10	1	5	5	1500	10.7	712.5	13.9
	2				12.5	693.5	15.9
	3				13.2	709.1	18.1
	4				11.8	420.7	16.2
	Average				12.0	634.0	16.0
11	1	1	22.5	2000	6.0	57.7	7.5
	2				5.9	63.9	7.3
	3				5.9	58.3	7.3
	4				7.9	90.8	9.9
	Average				6.4	67.7	8.0
12	1	1	40	1500	9.4	100.8	11.8
	2				9.9	96.7	12.2
	3				6.1	373.9	7.9
	4				11.3	96.7	13.9
	Average				9.2	167.0	11.5
13	1	5	22.5	1000	12.3	126.5	15.3
	2				11.7	120.9	14.6
	3				11.8	120.6	14.7
	4				13.0	137.6	16.1
	Average				12.2	126.4	15.2

Table G-1 (cont'd)

Run	Position #	Feed Rate	Depth of Cut	Spindle Speed	Ra	PV	rms
		($\mu\text{m}/\text{rev}$)	(μm)	(RPM)	(nm)	(nm)	(nm)
14	1	1	5	1500	3.9	53.6	4.9
	2				3.6	47.5	4.6
	3				3.4	44.2	4.3
	4				3.8	77.2	5.1
	Average				3.7	55.6	4.7
15	1	5	40	1000	13.6	426.0	16.9
	2				12.2	762.5	15.3
	3				12.8	121.4	15.9
	4				12.8	127.2	15.8
	Average				12.8	359.3	16.0
16	1	5	5	1000	10.4	132.7	13.1
	2				10.0	125.3	12.6
	3				9.9	101.4	12.4
	4				10.3	751.3	13.8
	Average				10.1	277.7	13.0
17	1	9	5	1000	11.5	740.2	17.0
	2				11.7	725.4	20.0
	3				11.3	978.7	20.6
	4				11.3	726.4	17.0
	Average				11.5	792.7	18.6
18	1	1	22.5	1000	8.5	102.6	10.7
	2				8.4	377.9	10.5
	3				8.4	85.3	10.5
	4				8.0	87.2	10.1
	Average				8.3	163.2	10.5
19	1	1	5	1000	3.9	57.5	5.1
	2				5.1	68.1	6.6
	3				4.9	72.8	7.1
	4				4.9	376.0	12.5
	Average				4.7	143.6	7.8
20	1	5	22.5	1500	8.6	406.3	11.3
	2				8.6	94.5	10.8
	3				8.4	93.8	10.5
	4				8.6	665.7	11.1
	Average				8.5	315.1	10.9

Table G-1 (cont'd)

Run	Position #	Feed Rate	Depth of Cut	Spindle Speed	Ra	PV	rms
		($\mu\text{m}/\text{rev}$)	(μm)	(RPM)	(nm)	(nm)	(nm)
21	1	5	40	1500	12.6	415.9	16.0
	2				13.3	713.2	17.0
	3				14.2	418.8	17.6
	4				14.3	410.5	19.5
	Average				13.6	489.6	17.5
22	1	9	40	2000	45.3	1491.9	97.2
	2				51.6	1366.6	99.4
	3				44.7	1719.4	95.9
	4				45.7	1683.9	97.3
	Average				46.8	1565.4	97.4
23	1	9	40	1000	27.4	1372.5	61.7
	2				25.0	1374.7	55.8
	3				24.9	1323.8	53.7
	4				26.3	1360.8	59.0
	Average				25.9	1357.9	57.6
24	1	1	22.5	1500	4.0	62.6	5.1
	2				4.3	49.6	5.5
	3				4.7	591.8	6.1
	4				4.1	41.8	5.2
	Average				4.3	186.5	5.5
25	1	9	40	1500	20.6	1407.9	45.7
	2				22.0	1401.3	48.8
	3				21.4	1408.9	49.4
	4				22.2	1429.9	51.1
	Average				21.6	1412.0	48.8
26	1	9	5	2000	19.3	1330.8	43.2
	2				24.5	1393.7	57.0
	3				27.1	1084.6	64.4
	4				17.4	1092.7	37.1
	Average				22.1	1225.4	50.4
27	1	9	22.5	1500	25.5	1398.5	61.2
	2				27.0	1720.1	63.5
	3				27.8	1382.4	65.3
	4				25.4	1385.6	61.0
	Average				26.4	1471.7	62.7

APPENDIX H

ALL SURFACE ROUGHNESS MEASUREMENTS FOR 8-RUNS VALIDATION EXPERIMENT

Table H-1 Surface Roughness Measurements for 8-runs validation experiment

Run	Position #	Feed Rate	Depth of Cut	Spindle Speed	Ra	PV	rms
		($\mu\text{m}/\text{rev}$)	(mm)	(RPM)	(nm)	(nm)	(nm)
1	1	2	3	1250	6.9	392.2	8.7
	2				6.4	86.0	8.2
	3				6.7	416.3	8.6
	4				7.6	90.9	9.5
	Average				6.9	246.3	8.7
2	1	7	22	1000	15.6	763.0	20.5
	2				17.8	796.6	28.5
	3				22.0	776.4	44.6
	4				17.0	787.5	27.3
	Average				18.1	780.9	30.2
3	1	12	10	1750	49.1	1688.0	100.4
	2				48.0	1724.4	98.9
	3				48.0	1677.4	95.8
	4				45.5	1473.4	91.3
	Average				47.7	1640.8	96.6
4	1	2	6	2250	6.2	79.5	7.9
	2				6.4	76.8	8.1
	3				6.3	87.3	7.9
	4				6.3	72.9	8.1
	Average				6.3	79.1	8.0

Table H-1 (cont'd)

Run	Position #	Feed Rate	Depth of Cut	Spindle Speed	Ra	PV	rms
		($\mu\text{m}/\text{rev}$)	(mm)	(RPM)	(nm)	(nm)	(nm)
5	1	7	30	1750	23.1	1158.8	43.4
	2				23.3	1081.2	43.4
	3				21.5	781.3	42.1
	4				24.1	1111.7	45.3
	Average				23.0	1033.2	43.5
6	1	12	40	1250	56.4	1944.1	113.9
	2				42.1	1711.4	88.8
	3				56.5	2024.1	114.6
	4				53.2	1742.8	109.4
	Average				52.1	1855.6	106.7
7	1	2	50	1000	6.1	69.8	7.7
	2				6.0	73.3	7.7
	3				5.2	82.9	6.8
	4				6.0	692.9	9.1
	Average				5.8	229.7	7.8
8	1	7	20	2250	14.7	1600.7	26.7
	2				14.1	732.4	21.6
	3				13.2	741.3	18.8
	4				15.5	749.0	26.6
	Average				14.4	955.8	23.5